JOURNAL OF GEOPHYSICAL RESEARCH, VOL. 106, NO. A4, PAGES 5779–5798, APRIL 1, 2001

Properties of large electric fields in the plasma sheet at 4-7 R_E measured with Polar

A. Keiling,[1] J. R. Wygant,[1] C. Cattell,[1] M. Johnson,[1] M. Temerin,[2] F. S. Mozer,[2] C. A. Kletzing,[3] J. Scudder,[3] and C. T. Russell[4]

Abstract. Measurements from the Polar satellite provide evidence for large electric field structures in the plasma sheet at geocentric distances of 4-7 R_E. These structures had amplitudes perpendicular to the ambient magnetic field that can exceed 100 mV m^{-1} (6 s averaged). Two years (from May 1, 1996, to April 30, 1998) of electric field data (E_Z component, approximately along GSE z) were surveyed. The distribution in invariant latitude (ILAT) and magnetic local time (MLT) of large perpendicular electric field events (defined as $\geq$20 mV m^{-1} for a 6-s average) delineates the statistical auroral oval with the majority of events occurring in the nightside centered around midnight and a smaller concentration around 1500 MLT. The magnitude-versus-altitude distribution of the electric fields between 4 and 7 R_E in the nightside could be explained by models which assume either shear Alfvén waves propagating into regions of larger background magnetic fields or electrostatic structures being mapped quasi-statically along equipotential magnetic field lines. In addition, this survey yielded 24 very large amplitude events with $|E_\perp| \geq$100 mV m^{-1} (6 s averaged), all of which occurred in the nightside. In the spacecraft frame, the electric field structures occurred on timescales ranging from 10 to 60 s. About 85% of these events occurred in the vicinity of the outer boundary of the plasma sheet; the rest occurred in the central plasma sheet. The polarity of the electric fields was dominantly perpendicular to the nominal plasma sheet boundary. For a large fraction of events ($\leq$50%) the ratios of electric and magnetic fields in the period range from 10 to 60 s were consistent with Alfvén waves. Large Poynting flux (up to 2.5 ergs cm^{-2}s^{-1}) dominantly directed downward along the background magnetic field was associated with 21 events. All 24 events occurred during geomagnetic disturbances such as magnetic substorms. A conjugate study with ground stations for 14 events (out of the 24 events) showed that these structures occurred during times of rapid changes in the H component (or X component) of magnetometer data. For most events this time corresponded to the expansion phase; two events occurred during a quick recovery of the negative H bay signature. Thus there is evidence that large electromagnetic energy transfer processes in the plasma sheet occur during the most dynamic phase of geomagnetic disturbances. From the statistical analysis it was found that Polar observed events larger than 100 mV m^{-1} (50 mV m^{-1}) in the plasma sheet between 2100 and 0300 MLT with a 2-4% (15%) probability per crossing. These probabilities will be compared to the probability of substorm occurrence during Polar plasma sheet crossings.

1. Introduction

The interest in large electric fields (perpendicular to the ambient magnetic field) on auroral field lines has existed since their first observation by *Mozer et al.* [1977]. It has been an ongoing issue in auroral physics to discover the origin of these fields, and to establish their role in auroral phenomena. Statistical studies of electric fields in and above the auroral zone made with data from S3-3 [*Mozer et al.*, 1977; *Bennett et al.*, 1983; *Redsun et al.*, 1985], ISEE 1 [*Mozer*, 1981; *Cattell et al.*, 1982; *Levin et al.*, 1983], DE 1 [*Gurnett et al.*, 1984; *Weimer and Gurnett*, 1993], Viking [*Lindqvist and Marklund*, 1990], and Freja [*Karlsson and Marklund*, 1996] have established that these fields are common from the ionosphere up to at least 23 R_E geocentric distance. Recent Geotail studies [*Cattell et al.*, 1994; *Streed et al.*, 2000] have shown that they can occur out to 100 R_E.

An important result from some of these studies [*Bennett et al.*, 1983; *Redsun et al.*, 1985; *Karlsson and Marklund*,

[1] School of Physics and Astronomy, University of Minnesota, Minneapolis.

[2] Space Sciences Laboratory, University of California, Berkeley.

[3] Physics Department, University of Iowa, Iowa City.

[4] Institute of Geophysics and Planetary Physics, University of California, Los Angeles.

Paper number 2000JA900130.
0148-0227/01/2000JA900130$09.00

1996] has been that the large perpendicular electric fields observed at altitudes between 1400 and 8000 km delineate the statistical auroral oval. This was evidence that the perpendicular electric fields in this altitude range were related, and led to the question of whether auroral electric fields measured at different altitudes result from mapping along equipotential magnetic field lines of electrostatic structures created, presumably, in the auroral acceleration region to altitudes of observation. *Mozer* [1981] and *Levin et al.* [1983] investigated this issue, and for geocentric distances greater than 4 R_E their results were consistent with the simple model in which the electric fields map quasi-statically to high altitude. The decrease in magnitude of the electric field values with altitude was explained through geometrical spreading of equipotential magnetic field lines. Deviations from this model at lower altitudes were interpreted as evidence for field-aligned potential drops [*Mozer et al.*, 1977; *Mozer*, 1981; *Weimer and Gurnett*, 1993]. Other theoretical studies [e.g., *Hasegawa*, 1976; *Goertz*, 1984; *Mallinckrodt and Carlson*, 1978] and observational case studies [e.g., *Dubinin et al.*, 1990; *Lotko and Streltsov*, 1997; *Wygant et al.*, 2000] have suggested that some of the electric field structures seen in the auroral zone and above could be caused by Alfvén waves, which are electromagnetic structures.

A region of great importance to auroral substorm physics is the plasma sheet boundary layer (PSBL). It is located between the tail lobes and the central plasma sheet (CPS), connecting the auroral acceleration region with the distant tail, where reconnection processes have been invoked [*Baker et al.*, 1996, and references therein]. The determination of the structure of the PSBL has been an important issue in magnetospheric physics, because the PSBL is intrinsically linked to auroral phenomena. With respect to the electric field the structure of the boundary in the magnetotail has been explored by the ISEE satellites [*Cattell et al.*, 1982; *Pedersen et al.*, 1985; *Parks et al.*, 1984] at 7-23 R_E geocentric distance and by Geotail [*Cattell et al.*, 1994; *Streed et al.*, 2000] up to 100 R_E. A recent Polar study by *Wygant et al.* [2000], who examined large perpendicular electric fields ($\geq$ 100 mV m^{-1}) and associated magnetic field fluctuations in the PSBL at geocentric distances of 4-6 R_E during two plasma sheet passes, showed that the fields were consistent with Alfvén waves carrying large Poynting fluxes (1-2 ergs cm^{-2}s^{-1}, in situ) along the magnetic field toward the ionosphere, and that the fields were magnetically conjugate to intense auroral structures.

In this paper we will present the first statistical study of electric fields in the high-altitude Northern Hemisphere covering the period from May 1, 1996, to April 30, 1998, using data from the Polar satellite. We examined low-resolution spin-averaged data ($\leq$1/6 Hz). Only the component perpendicular to the ambient magnetic field was considered. The dependence of the electric field on magnetic local time (MLT), invariant latitude (ILAT), and geocentric distance was investigated. This study complements previous statistical studies by making use of Polar's unique orbit and attempts to shed further light on the spatial distribution, occurrence frequency, and mapping characteristics of perpendicular electric fields on auroral field lines. Polar is placed in an 18-hour polar orbit (80° inclination), with perigee and apogee of 2.2 and 8.5 R_E, respectively. Hence it offers the opportunity to examine the plasma sheet and its poleward boundary at geocentric distances of 4-7 R_E, a region which is intermediate between the auroral acceleration region ($\sim$1-3 R_E) and the more distant portions of the magnetotail. A study of this region is relevant for processes in the auroral acceleration region and in the magnetotail. In addition to the large database statistical study, a case study of the largest perpendicular electric fields (defined as $\geq$100 mV m^{-1}) measured by Polar was done. Twenty-four of such events were found during the 2-year time period of the statistical study. In $\sim$85% of the cases the satellite encountered the largest of the electric fields in a localized region near the lobe-PSBL interface; the remaining events were found further into the plasma sheet. As examples of large-amplitude events, we present three Polar passes which showed very large perpendicular electric fields in the PSBL at geocentric distances of 4.5-6 R_E. Inspection of the E-to-B ratios of the perturbation fields give evidence that a large fraction ($\leq$50%) of the largest events ($|E_\perp| \geq$100 mV m^{-1}) are of Alfvénic nature. The majority of events (21 events) were associated with strong earthward Poynting flux. Furthermore, a temporal comparison of 14 of the largest Polar events with ground magnetometer records is presented. The ground data allowed us to place the spacecraft data into the context of the overall substorm system. One important conclusion from this comparison is that these events were associated with geomagnetic disturbances such as substorms occurring in close temporal proximity to substorm onset or intensification.

2. Instrumentation

In this study we used Polar spacecraft data from the University of California (UC) Berkeley Electric Field Instrument [*Harvey et al.*, 1995], the University of Californaia at Los Angeles (UCLA) Fluxgate Magnetometer [*Russell et al.*, 1995], and the University of Iowa Hydra Plasma Instrument [*Scudder et al.*, 1995]. The electric field is determined from a measurement of the electric potential difference between pairs of current-biased spherical sensors. These sensors are deployed at the ends of three orthogonal pairs of booms with tip-to-tip separations of 100 and 130 m (in the spin plane) and 13.8 m (along the spin axis). The three-axis electric field vector is sampled at 20 samples per second (sometimes at 40 samples per second). For the statistical analysis, only data from the sensors in the spin plane, which is approximately aligned with the local meridional plane, were used. For other parts the full three-dimensional electric field vector was used. The magnetic field vector is sampled at $\sim$8.3 samples per second by the three-dimensional fluxgate magnetometer. The particle detector provides measurements of electron and ion energy flux at 1.2- and 12-s time resolutions, of which the latter is used in this study, in the energy range from 12 eV to 18 keV.

In addition to Polar data, we utilized magnetometer data from ground stations to determine substorm phases. The

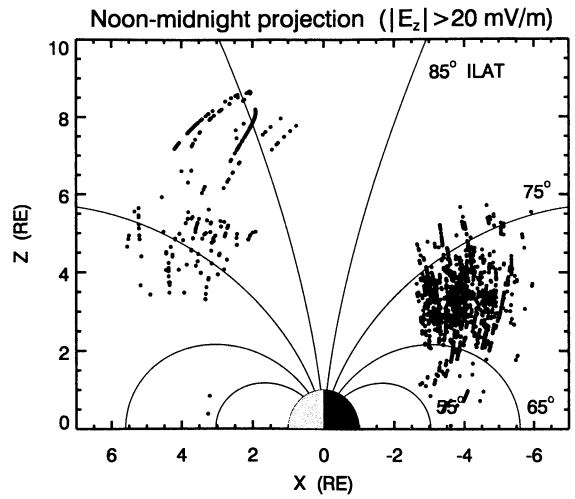

Figure 1. Projection of electric field events with perpendicular amplitude larger than 20 mV m^{-1} occurring between 0900 and 1500 MLT and between 2100 and 0300 MLT onto the noon-midnight plane (Northern Hemisphere).

ground magnetometer data were taken from four magnetometer arrays: the Canadian Auroral Network for the Open Unified Study (CANOPUS), the Magnetometer Array for Cusp and Cleft Studies (MACCS), the 210 degree Meridian Chain (210MM) [*Yumoto et al.*, 1996], and the International Monitor for Auroral Geomagnetic Effects (IMAGE).

3. Data Analysis

The electric field data used for this study were obtained from key parameter data and high-resolution data (20 and 40 samples per second). The electric field in the key parameter database is computed once per spin period (6 s) applying sine wave spin fits to the electric fields measured in the spacecraft spin plane. For the statistical part of this study, we used the E_Z component which points north (approximately along GSE z), and at geocentric distances of 4-7 R_E on Polar's orbit it is approximately perpendicular to the ambient magnetic field and the nominal plasma sheet boundary. Since E_Z is not always exactly perpendicular to the ambient magnetic field, the value of the full perpendicular component is slightly underestimated. A database was constructed from the key parameter database by determining the largest electric field in each 30-s interval. This database was used to generate distribution plots for the electric field as functions of ILAT, MLT, and geocentric distance. Only data obtained at locations with ILAT between 50° and 90° (Northern Hemisphere) were included. During the period from May 1, 1996, to April 30, 1998, the Polar spacecraft completed ~940 orbits and twice as many auroral zone crossing in the northern hemisphere, resulting in about 1.7 million event entries in our database. Note that for different parts of this study, subsets of the database were used, which will be indicated when appropriate.

A typical pass of Polar across the northern hemisphere shows large perpendicular electric fields ($\geq$20 mV m^{-1}) in the plasma sheet and in the cusp. This is illustrated in Figure 1, which shows a projection onto the noon-midnight plane of electric field events with amplitudes larger than 20 mV m^{-1} occurring between 0900 and 1500 MLT, and 2100 and 0300 MLT as a function of radial distance and magnetic latitude. The bulk of the data in the nightside occurred on auroral field lines between 65° and 75° and between 4 and 7 R_E geocentric distance. Dayside electric field observations occurred at higher latitude and larger geocentric distances. The altitude range varies because of Polar's elliptical orbit. For most parts of this study, we characterized electric fields on auroral field lines in the nightside (more detail is given in section 4).

The electric fields inside the plasma sheet and the cusp are highly variable. An example of a plasma sheet crossing observed by Polar on August 29, 1997, during an outbound pass from the equatorial plane to the tail lobe is given in Plate 1. Plates 1a and 1b show the two components of the electric field measured in the spin plane of the satellite. The E_X component of the electric field is approximately in the ecliptic plane, with positive values in the direction away from the Sun. The E_Z component points northward and perpendicular to the ecliptic plane (approximately along GSE z). Plate 1c shows the east-west perturbation from the ambient magnetic field. This component lies approximately in the plane of the nominal plasma sheet. Plate 1d shows the electron density determined from the Hydra particle detector. Plates 1e and 1f show the energy spectra of ions and electrons. The intensity is color-coded with red representing the highest intensity and blue representing the weakest.

During the pass on August 29, 1997, the satellite encountered the inner edge of the plasma sheet at ~ 0950 UT, indicated by the gradual, dispersive-like increase of ion and electron energy up to plasma sheet values. The crossing of the entire plasma sheet lasted for ~40 min, during which Polar encountered two field-aligned current sheets of opposite direction and one "bipolar" electric field structure (~40 mV m^{-1} at 1020 UT). At ~1033 UT, Polar most probably crossed the lobe-PSBL interface, entering a low-energy electron region, known as polar rain [*Winningham and Heikkila*, 1974]. Polar rain is an indicator for open field lines and extends across the polar cap. At ~1037 UT the satellite reentered the plasma sheet, inferred from the abrupt increase in the ion and electron fluxes to plasma sheet values. This interpretation as opposed to a spatially structured plasma sheet is further supported by Polar measurements of the other two magnetic field components (meridional components, not shown) and the GOES-9 satellite (not shown), indicating a dipolarization around 1037 UT and 1032 UT, respectively. This dipolarization caused an expansion of the outer edge of the plasma sheet, which swept by the satellite. Polar remained in the plasma sheet until around 1200 UT, when it again entered the lobe region, indicated by low-energy electrons and no visible ions in the Hydra measurements (similar to the first leaving of the plasma sheet at ~1033 UT). It is interesting to note that the first and second crossings of the lobe-PSBL interface occurred at very different values of ILAT, namely, ~67° and ~75°, respectively. This re-

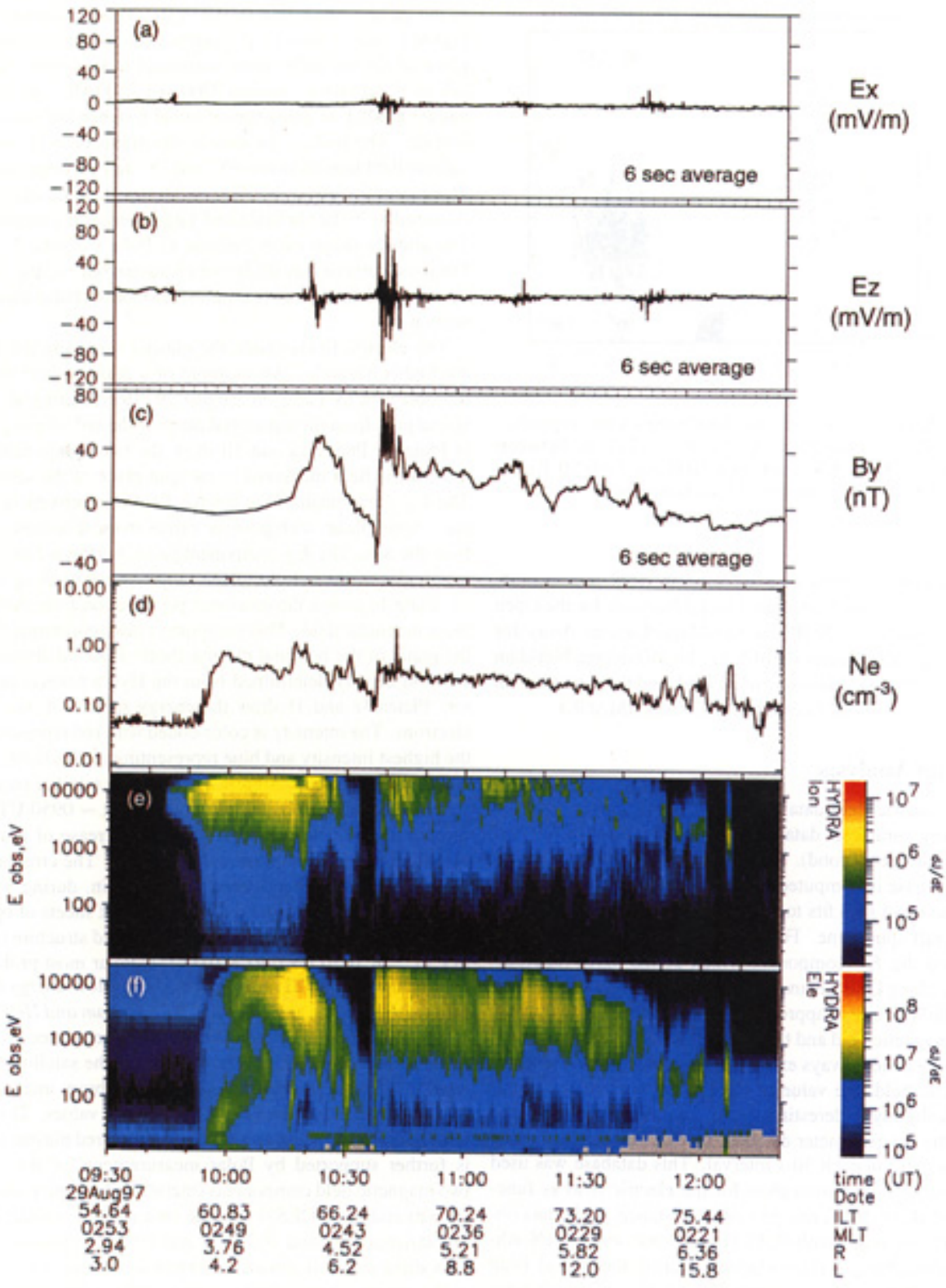

Plate 1. Plasma sheet crossing on August 29, 1997, showing large-amplitude electric fields. (a,b) Two electric field components in the spin plane of the satellite (E_X is approximately in the ecliptic plane, with positive values in the direction away from the Sun; E_Z points northward and perpendicular to the ecliptic plane, approximately along GSE z), (c) the magnetic field perturbation from the ambient field (pointing east-west), (d) the electron density, and (e,f) energy-time spectrograms of ions and electrons. The satellite left the plasma sheet for the first time at ~1033 UT, shortly after which it reentered the plasma sheet at ~1037 UT.

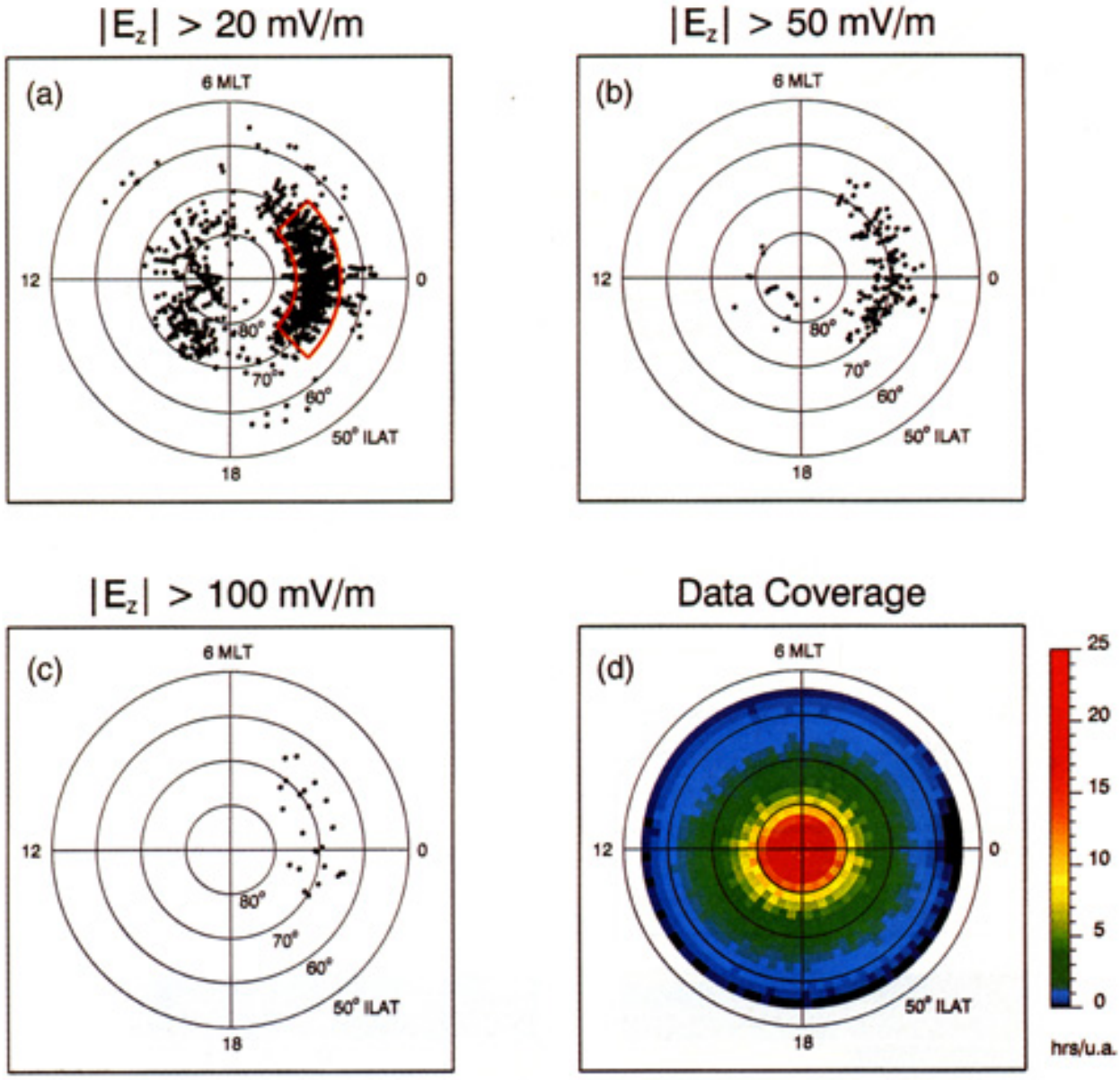

Plate 2. Distribution of electric field events as a function of ILAT and MLT for values with (a) $|E_Z| \geq 20$ mV m^{-1}, (b) $|E_Z| \geq 50$ mV m^{-1}, and (c) $|E_Z| \geq 100$ mV m^{-1}. The box outlined in Plate 2a indicates the region that is used for other parts of the statistical analysis. (d) The data coverage by the Polar satellite. The color scale indicates the time spent per unit area.

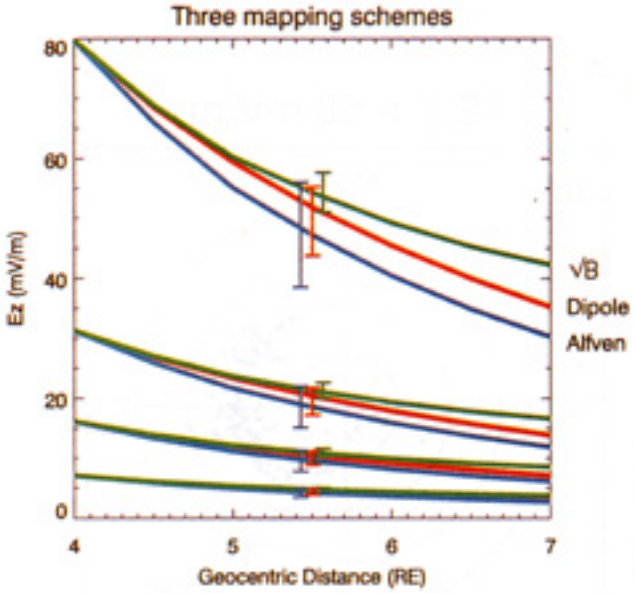

Plate 3. Comparison of three mapping schemes. The red (green, blue) curves are calculated from equation (1) (equation (2), equation (3)). The reference values (interception of curves) were chosen to be the same for all schemes (see text for description).

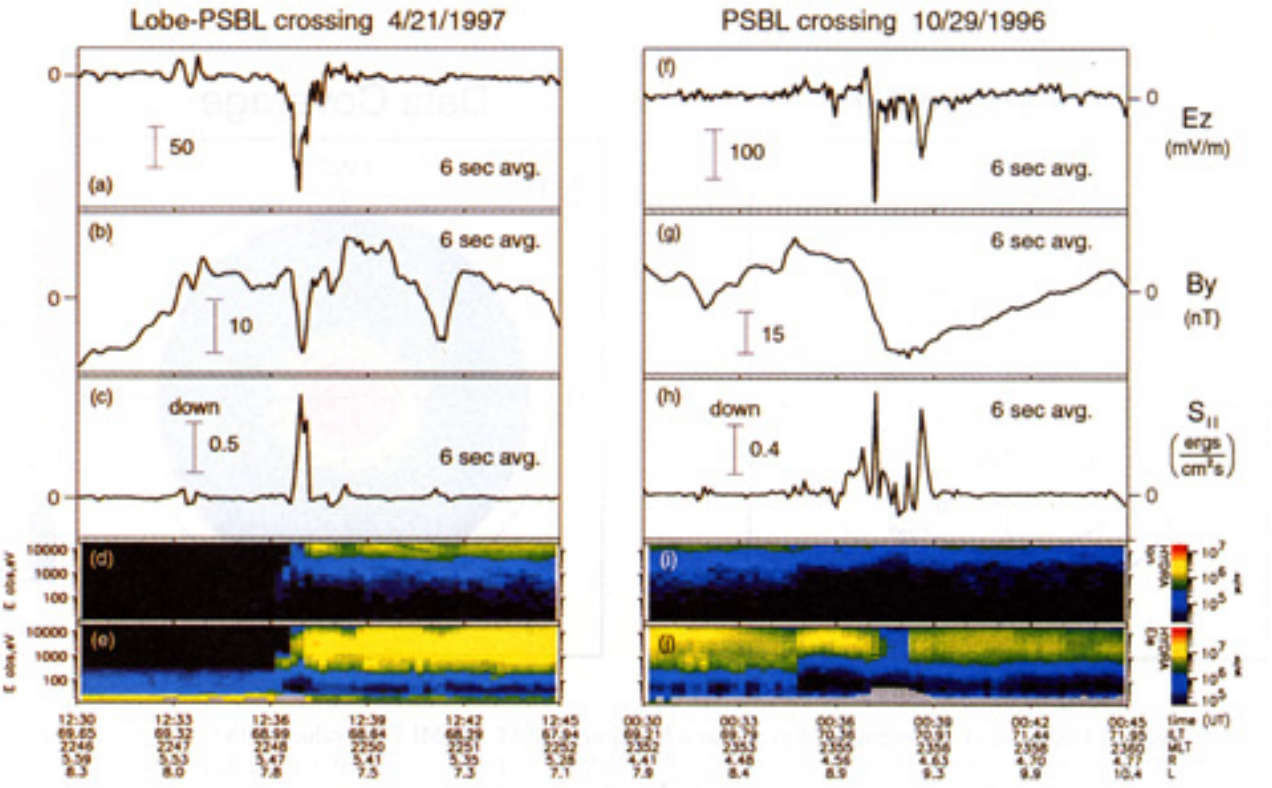

Plate 4. Two PSBL crossings which showed large-amplitude perpendicular electric fields. (a-e) From top to bottom, one electric field component (approximately along GSE z; 6 s averaged), the west-east component of the magnetic field (model subtracted; 6 sec averaged), the Poynting flux associated with electric and magnetic field perturbations (see text for description), and energy-time spectrograms of ions and electrons. (f-j) Same as in Plates 4a-4e but for October 29, 1996.

flects the well-known thinning and expansion of the plasma sheet [e.g., *Baumjohann et al.*, 1992]. This interpretation also agrees well with ground observations for this event (presented in section 5.4), indicating substorm expansion and recovery phases during the time of the plasma sheet crossing.

The second entry of the plasma sheet at 1037 UT coincided with a density jump of the electrons from 0.1 to 0.4 cm^{-3}, and a downward current sheet as indicated by the shift in the dc level of B_Y (Plate 1c). The current sheet was carried over Polar owing to the rapid dipolarization. It most likely is the same current sheet that was encountered before Polar left the plasma sheet at ~1033 UT. Because of the relative motion of the boundary and the satellite, the slope of B_Y is in the opposite direction. After plasma sheet entry, Polar encountered a localized region of large electric field fluctuations, lasting for a period of ~5 min in the spacecraft frame. Within this region, high-resolution measurements provide evidence for spiky electric fields with amplitudes ranging up to 300 mV m^{-1} and durations of 1/10-1 s (not shown). These rapid time variations were superimposed on the slower varying signal with amplitudes of up to 120 mV m^{-1} (6-s average). The electric field structure also coincided with strong magnetic field fluctuations. For the remaining crossing of the plasma sheet (until ~1200 UT), Polar recorded much smaller electric fields ($\leq$30 mV m^{-1}).

Furthermore, a computer search was conducted that recorded all events for which the E_Z component of the electric field exceeded an amplitude of 100 mV m^{-1}. The plasma regions for these events were determined by inspection of particle data (Hydra). For 14 out of the 24 events, we identified ground stations close to Polar's magnetic footpoint at the event times. The ground data were used to establish a temporal relationship between Polar's large electric field observations and substorm onset/intensification. Only the unfiltered H (or X) component, depending on which magnetometer chain was used, is presented, because it is this component which responds strongest to the substorm electrojet. This component is routinely used as an indicator of substorm onset/intensification. The X component points to geographic north whereas the H component points to geomagnetic north. The sampling rate of the ground data was different for different magnetometer chains, ranging between one sample per second and one sample per minute. K_P and AE indices (preliminary; no AE index values were available for 1996) were also consulted to put these large-amplitude events into a global geomagnetic activity context.

4. Statistical Results

4.1. Location of Events

Plate 2 presents distributions of electric field events versus ILAT and MLT obtained from the database described in section 3. Plate 2a (Plates 2b and 2c) shows the distribution of events whose perpendicular electric field component (E_Z) as measured by Polar exceeds 20 mV m^{-1} (50 mV m^{-1}, 100 mV m^{-1}). A dipole field was assumed for the mapping onto ILAT. Note that the data were not normalized to account for a possible undersampling of certain regions in the longitudinal (MLT) direction. This was not necessary because Polar's orbit precesses once a year, and since the study covers exactly 2 years, each MLT was roughly visited 4 times. The uniform data coverage along MLT is shown in Plate 2d. The region with ILAT$\geq$50° is divided into many small "squares." The time spent by Polar in each square was divided by the size of the square to remove biases caused by small differences in square size. The color code thus represents the data coverage in units of time/(unit area) with red representing more hours and blue representing less. The actual time spent is not important here, but rather the uniformity in the longitudinal direction.

Almost all electric field events were located within the statistical auroral oval, which is centered several degrees antisunward of 90° with a few events occurring inside the statistical polar cap. The distribution along the auroral oval is not uniform. The dayside events were less intense than the nightside events, which can be seen by comparing the panels with higher electric field thresholds. Events with $|E_Z| \geq$20 mV m^{-1} (Plate 2a) are symmetrically distributed around the noon-midnight meridian on the nightside. On the dayside one can identify a small concentration around 1500 MLT, which coincides with the so-called hot spot [*Evans*, 1985; *Newell et al.*, 1996]. Events larger than 50 mV m^{-1} (Plate 2b) occurred mostly on the nightside, with a few more events in the morning sector and covering a wider range of ILAT. Events larger than 100 mV m^{-1} (Plate 2c) occurred only in the nightside, similarly distributed as the events larger than 50 mV m^{-1}. The total number of such events, however, is statistically not significant to conclude that the morningside has a higher probability for the largest events. There are two 2-hour wide regions on the dawnside (~0500 MLT) and duskside (~1900 MLT) which show significantly lower event rates than the surrounding regions. An investigation of the data coverage (Plate 2d) shows minimal variations in the longitudinal direction which cannot account for the two regions of low-event rate.

4.2. Altitude Dependence

For the rest of the statistical analysis we only consider events in the region defined by 65°$\leq$ILAT$\leq$75° and 2100 $\leq$MLT$\leq$0300 (box outlined in Plate 2a) in order to characterize perpendicular electric fields on auroral field lines in the nightside. We chose this region because it encompasses a relatively uniform distribution of events including the largest events. Also, the cutoffs at 65° and 75° ILAT correspond approximately to the range of PSBL locations during times of different geomagnetic activities (compare August 29, 1997, event in Plate 1). This database contains 87,444 events (as defined in section 3).

Figure 2 shows a scatterplot of electric field events versus geocentric distance. Considering only the largest events (with $|E_Z| \geq$100 mV m^{-1}), one can conclude that the magnitude decreases with increasing altitude. However, the small number of events larger than 100 mV m^{-1} is statistically not significant. Therefore we considered contour

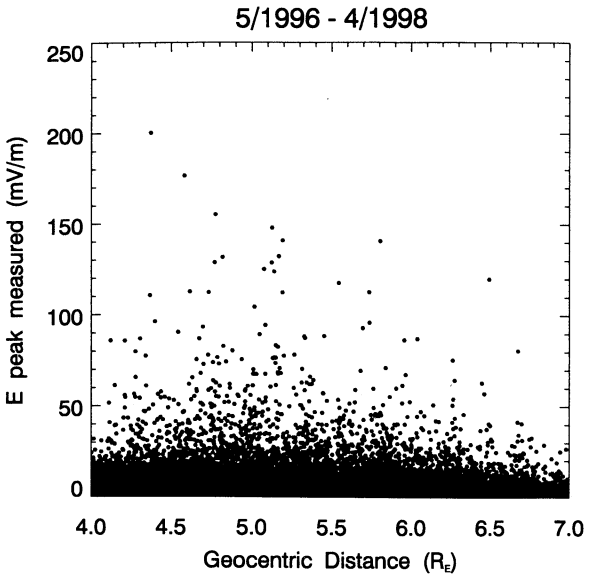

Figure 2. Distribution of in situ electric field events plotted versus geocentric distance. The events are those that lie between 65°≥ILAT≥75° and 2100≤MLT≤0300 (box outlined in Plate 2a).

curves, which is described in the next paragraph, to analyze the magnitude-versus-distance distribution. The main interest in the magnitude-versus-distance distribution has been in establishing a mapping relationship for perpendicular electric fields at different altitudes. In the literature, two approaches have been taken to investigate the mapping relationship. They are both derived from the assumption of quasi-static electric fields and equipotential field lines (called static model hereinafter). The first relation is based on a dipole magnetic field geometry [*Mozer*, 1976]. The electric field maps to different altitudes according to

$$E = E_0 \left(\frac{4L - 3r}{4L - 3r_0} \right)^{\frac{1}{2}} \left(\frac{r_0}{r} \right)^{\frac{3}{2}} , \qquad (1)$$

where L is the L value of the magnetic field line, and E and E_0 are the mapped electric fields along the magnetic field line at altitudes r and r_o, respectively. E_0 and r_0 are reference values. When leaving the dipole region, it is better to use the relation

$$E \propto \sqrt{B} , \qquad (2)$$

where B is the local magnetic field strength. We have applied both relationships to the Polar data. In addition, we tested the database under the assumption that the observed electric fields are the perturbation fields of shear Alfvén waves. This has never been done with a large amount of data at altitudes of 4-7 R_E. If one assumes that the power flow, $(A/\mu_0)\delta E \times \delta B$, carried by the shear Alfvén wave with electric (δE) and magnetic (δB) perturbation fields along a flux tube with cross section, A, is conserved (see section 6 for exceptions), one can derive, using also the Alfvén speed, $v_A = \delta E/\delta B$, and conservation of magnetic flux ($BA = const$ along the flux tube),

$$\delta E \propto \sqrt{v_A B} . \qquad (3)$$

Note that if there are parallel potential drops present, none of the three relationships hold. However, other studies [e.g., *Reiff et al.*, 1993] have established, using particle energies and hence not relying on mapping along magnetic field lines, that most field-aligned potential drops occur below 15,000 km (3.35 R_E geocentric distance), which is below the altitude range considered in the study presented here.

In order to make a more statistically significant test of the three models, we generated contour curves from the scatterplot (Figure 2). A 1% contour curve, for example, shows the value of the electric field such that 1% of the events within a certain altitude range (here we chose 0.5 R_E) have a value larger than the plotted value. Contour curves eliminate the weakness of scatterplots, which is a reliance on only the largest values for a given altitude. Figure 3a shows four contour curves (0.5, 1, 5, and 20%) each of which was calculated from the same original database. For each curve the magnitude of the electric field decreases with increasing altitude. Also, as expected, the error bars are smaller for the larger percentage contour curves. The lower (upper) value of the error bars shows the electric field value of the event, which is obtained after sorting all events in a certain altitude range according to magnitude and selecting the event which precedes (follows) the plotted event by $\sqrt{n_t}$ events (n_t is the total number of events in this altitude range).

In comparison, Figure 3b shows four curves calculated from the model equation (1). Each curve shows the theoretical variations of the magnitude of an electric field, which maps quasi-statically along magnetic field lines in a dipole field to different altitudes. The electric field value (E_0 in (1)) used as reference for each curve was the first data point to the left of the corresponding contour curve in Figure 3a. The error bars in the model curves result from the uncertainty in L value. Since the plasma sheet location fluctuates with geomagnetic activity, we can only estimate that the L value lies between 65° and 75° ILAT. A comparison of the curves in Figures 3a and 3b clearly shows that within the range of statistical uncertainties, the data and model are consistent.

In addition to (1), Plate 3 shows model calculations using the other two equations, (2) and (3). We selected again the first data point to the left for each curve of Figure 3a as the reference electric fields, and we calculated the theoretical electric field values for higher altitudes. Each color represents a different mapping scheme defined by (1), (2), and (3). Equation (2) requires the knowledge of the local total magnetic field strength. Using the magnetic field data in the key parameter database, the mean value of the total magnetic field values (calculated from the three-dimensional magnetic field vector at times of all recorded electric field events in a given altitude bin) was computed and used in (2) to calculate the electric field value. The error bars of the green curves are the standard deviations of the electric field values calculated from the standard deviation of the magnetic field applied to the usual error propagation formula. Equation (3) requires knowledge of the local Alfvén speed. For 41 events (half of which had $|E_Z| \geq 50$ mV m^{-1}; the other half was ≤ 50

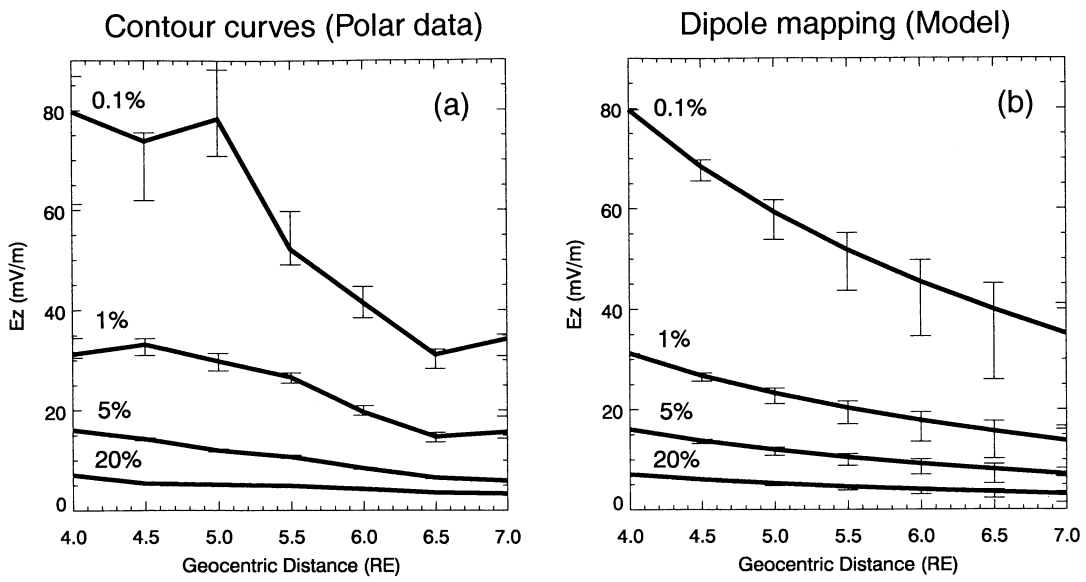

Figure 3. Comparison of Polar data and model calculations regarding the altitude dependence of electric fields. (a) Four contour curves (0.5, 1, 5, and 10%) calculated from the data shown in Figure 2. (b) Calculation of quasi-statically mapped electric fields in a dipole magnetic field using equation (1). The first data points to the left of each contour curve in panel (a) were used as reference values (see text for further description).

mV m^{-1}), we calculated the Alfvén speed from density data (Hydra), assuming 100% H^+, and magnetic field data. As can be seen in Figure 4, the Alfvén speed varied up to a factor of 2 at the same altitude. To calculate the theoretical electric field values at different altitudes, we applied a linear function for v_A, indicated by the solid line, in (3). For the blue curves, the variations in the Alfvén speed, v_A, were included in the error calculations. Although the three mapping schemes show deviations, within the range of the statistical uncertainties, they are indistinguishable. This shows that the consistency with the static model (as already shown by other researchers) does not rule out consistency with the Alfvén wave model in a statistical sense.

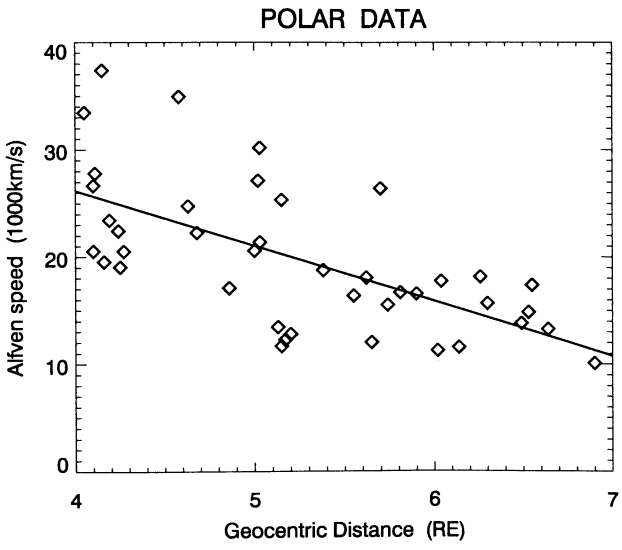

Figure 4. The local Alfvén speed, v_A, in the plasma sheet, associated with 41 randomly selected events of the electric field database, calculated from in-situ measurements of the field and plasma parameters.

4.3. Occurrence Frequency

We next examine the question of how often large-amplitude electric fields occur. Again, we only consider the region outlined by the box in Plate 2a. Figure 5 shows the probability distribution of electric field events within the defined region as a function of magnitude. The reader is reminded that the amplitude of an event is determined by the largest of five electric field measurements in a 30-s bin. The electric fields are grouped into bins of 10-mV m^{-1} width. Because of the large differences in probability for different electric field magnitudes, the probability distribution is displayed in two panels. The scale on the left of each panel shows probabilities calculated by dividing the number of events in each electric field bin by the total number of events. The probabilities for $|E_Z| \leq 10$ mV m^{-1} and 10 mV $m^{-1} \leq |E_Z| \leq 20$ mV m^{-1} are 0.936 and 0.047, respectively. They are not shown in Figure 5 which starts at $|E_Z| \geq 20$ mV m^{-1}. The general trend is that the probability decreases monotonically with increasing electric field magnitude. Used as a probability model, the probabilities in Figure 5 (left scale) allow the drawing of statistical conclusions. It might, for example, be useful to know how probable it is that Polar encounters at least one electric field structure with a certain amplitude during one entire plasma sheet crossing. These probabilities were calculated (using the probability model) and are shown on the right of each panel in Figure 5. Note that this scale is not linear. For example, the probability that Polar encoun-

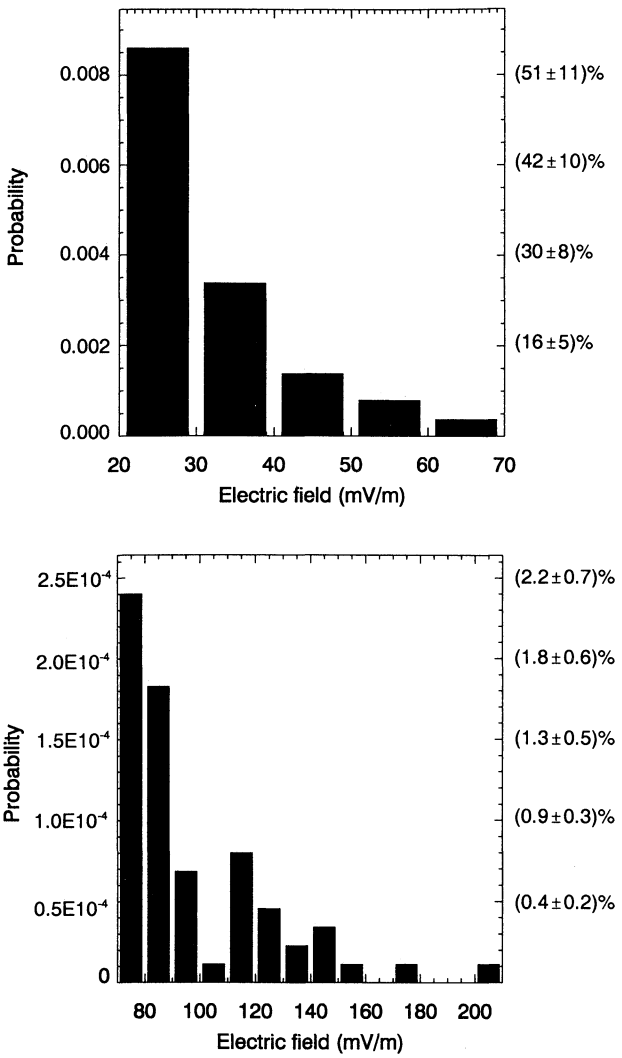

Figure 5. Probabilities of electric field events as a function of the electric field value. The events are those that lie between 65°≤ILAT≤75° and 2100≤MLT≤0300 (box outlined in Plate 2a). The electric field data were grouped into bins of 10 mV m^{-1} width. The left scale shows the probability of an event occurrence within the defined region. The right scale shows the probability of observing at least one event within a certain 10 mV m^{-1} bin per Polar plasma sheet crossing (see text for further description).

tered at least one event with perpendicular electric field amplitude between 40 and 50 mV m^{-1} during one entire plasma sheet crossing was ~14%±4%. The calculated uncertainties in the probabilities (right scale) result from the fact that Polar's crossing time of the entire plasma sheet varied between 30 and 60 min for different crossings (determined from visual inspections of ~40 crossings).

In section 5, it is shown that events with $|E_Z| \geq 100$ mV m^{-1} are substorm-related. Therefore it is also interesting to know how often these very large fields occur. Plate 2c shows that 24 events were recorded over a period of 2 years. An alternative way of quantifying their occurrence frequency is by using the probability model of Figure 5. One can show that the probability of observing an electric field larger than 100 mV m^{-1} within the outlined region (Plate 2a) is ~2% per plasma sheet crossing. Similarly, one can show that the probability of observing an electric field larger than 50 mV m^{-1} is ~15% per plasma sheet crossing. Instead of using the probability model, a simple calculation using the number of Polar orbits crossing the defined region during 2 years (~475 orbits) and the number of electric field events (≥100 mV m^{-1}) yields a probability of 4%, which is comparable to 2%. These probabilities will be compared to the probability of substorm occurrence during Polar plasma sheet crossings in section 6.

5. Substorm-Related Electric Fields

A computer search of the entire database yielded 27 events that showed perpendicular electric fields of more than 100 mV m^{-1}. All of these events were located in the nightside plasma sheet between 2100 and 0500 MLT (Plate 2c). A visual inspection of field and particle data showed that they occurred during 24 plasma sheet crossings. During three plasma sheet crossings, two (instead of one) large electric field pulses (≥100 mV m^{-1}) separated by 1-3 min were recorded. In the remainder of this paper we refer to these pairs as single events, thus yielding a total of 24 events.

A region of electric field fluctuations (≥5 mV m^{-1}) surrounding the most intense structures was usually observed, that lasted for ~5-30 min in the spacecraft frame. The region of most intense fluctuations (≥50 mV m^{-1}) lasted for ~1-5 min. Individual electric field pulses occurred on timescales of 10-60 s. Most of the 24 events revealed electric fields larger than 300 mV m^{-1} in the high-resolution electric field data. The geomagnetic activity during these events ranged from quiet to highly active, with the K_P index and the AE index (preliminary; no data available for 1996) taking on values between 0+ and 5+ and between ~40 and ~1100 nT, respectively. Although the AE index was ≤100 nT for two events (it was ≥150 nT for the remaining events), an inspection of magnetograms from individual ground stations near Polar's magnetically conjugate footpoint during these two events indicated geomagnetic activity as well. This will be shown in more detail in section 5.4. Hence we can conclude that geomagnetic disturbances such as substorms were present during all 24 events.

5.1. Plasma Regimes

In ~85% of the events the large electric field structure was found at or near the poleward boundary of the plasma sheet (i.e., the PSBL). The other events occurred deeper inside the plasma sheet. For some events, Polar may have encountered the lobe-PSBL interface more than once, which led to uncertainties as to whether the event occurred inside the PSBL or CPS. The different plasma regimes were identified by examining the particle data from the Hydra instrument. The lobe-PSBL interface can be identified by a flux increase (in the direction of decreasing ILAT) of ions and electrons accompanied by a density increase of ions and electrons. The width of the region over which the fluxes increased varied

considerably in the spacecraft frame. For some plasma sheet crossings, one of which is presented in section 5.5 (Plates 4a-4e), the flux increase occurred abruptly, less than 2 min in the spacecraft frame. In these cases the large-amplitude electric fields were located immediately adjacent to the lobe-PSBL interface on the higher-density side. For other plasma sheet crossings, particle fluxes gradually increased with decreasing ILAT (up to 30 min in the spacecraft frame). In those cases the largest electric field fluctuations were located further into the PSBL. Similar particle flux signatures have been reported for low-altitude satellites [e.g., *Lyons*, 1991].

Another often used distinction between PSBL and CPS is whether the particle flux is structured or unstructured, respectively. On the basis of this criterion, we identified some events as occurring inside the CPS. Four events also coincided with a very localized reduction (dropout) of the electron flux (an example is presented in section 5.5, Plates 4f-4j). In a few cases we interpreted a particle flux dropout as a crossing of the lobe-PSBL boundary into the lobe region, followed by a reentering of the PSBL due to an expanding plasma sheet. Plate 1 shows an example where we believe that this scenario is correct. The dropout lasted longer, and the electron energy reached values that are typical for tail lobe electrons. Alternatively, a large dropout could be due to a spatially structured plasma sheet rather than a temporal variation caused by the motion of the PSBL. On the basis of 24 events, the outer boundary location ranged from 65° to 78° ILAT, which supports the idea that multiple encounters of the lobe-PSBL interface during one pass are probable.

5.2. Polarization

The large-database statistical study presented in section 4 was based only on the E_Z component. This component is approximately perpendicular to the nominal plasma sheet boundary at the altitude range investigated here. The east-west component was not included. A knowledge of the east-west component, however, is important for investigating the origin of the very large electric fields. Hence we used (for this analysis only) electric field data in a magnetic-field-aligned coordinate system, in order to determine the dominant direction of the perpendicular component of the large electric field structures. The two components are Ey_FAC (east-west) and Ex_FAC (approximately the same as E_Z). The results of this analysis are shown in Figure 6, which shows the ratios of Ey_FAC over Ex_FAC, binned by their percentage values. The value, used for Ey_FAC, was the largest value observed within 2 min surrounding the largest value in Ex_FAC. For the majority of events (18 events) the amplitude of the east-west component was less than 40% of that of the north-south component.

5.3. Association With Field-Aligned Currents

The large electric fields occurred in regions of large-scale field-aligned currents (~1° ILAT) inferred from magnetic field measurements. Preliminary results show that seven events were associated with upward currents, four in the evening sector and three in the morning sector of magnetic

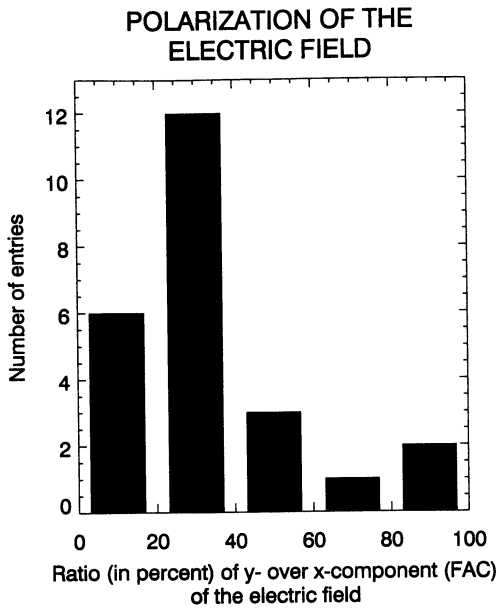

Figure 6. Comparison of the magnitudes of the two perpendicular electric field components (east-west and north-south) for the 24 largest electric field events found during 2 years of Polar operation.

local time. Events associated with downward currents were only found in the morning sector (four events). Note that these results include only events for which an identification of the current was straightforward. The current signatures for the remaining events were more complicated, and an association with a particular direction of current flow was ambiguous. A forthcoming study will show these results in greater detail.

5.4. Conjugate Study With Ground Stations

For a subset of 14 events, ground magnetometer data were examined in order to determine the temporal relationship of these events to different substorm phases. The ground stations were selected on the basis of being in the general proximity of Polar's magnetically conjugate footpoint. For some events, which occurred at 0200-0300 MLT, and for which no conjugate ground stations (or data) were available, we instead consulted ground stations that were close to local midnight. The substorm on August 29, 1997 (see next paragraph), shows that substorm ground signatures can extend over many hours local time; thus the latter selection criterion seems to be a reasonable alternative.

In general, the substorm onset time coincides with the beginning of a sharp negative turning of the H (or X) component detected at individual ground stations. This is the begin of the expansion phase. This phase is followed by the recovery phase identified as a gradual retreat of the H (or X) component to its original values. Often, however, the recovery phase is superimposed by additional intensifications. The ground data for the 14 events presented here fit roughly into this scheme.

We first present two Polar events which took place on August 29, 1997, and April 21, 1997, together with ground data.

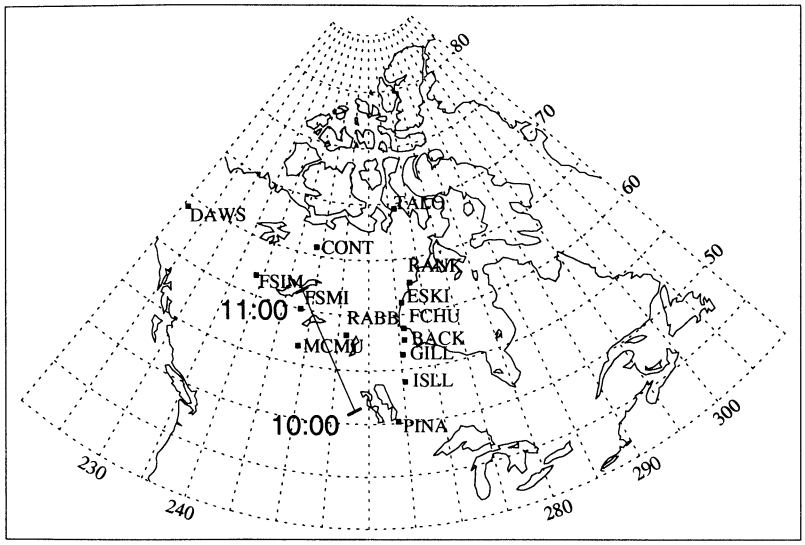

Figure 7. The geographic locations of the Canadian Auroral Network For the Open Unified Study (CANOPUS) stations. The solid line indicates Polar's magnetic footpoint on August 29, 1997, from 1000 to 1100 UT.

Additional Polar data for the August 29, 1997, event were already presented in Plate 1. *Toivanen et al.* [2000] have also investigated this event with regard to substorm onset signatures in the plasma sheet. Polar's magnetic footpoint traversed the CANOPUS array, which is shown for the period from 1000 to 1100 UT on August 29, 1997, in Figure 7, together with the geographic location of the ground stations. Figure 8 shows the X component of the CANOPUS stations for which data were available. A strong substorm bay signature can clearly be seen in all ground stations (with the exception of Contwoyto Lake (CONT)), starting at ~1035 UT. This agrees with the onset time determined from the AE index. The magnetogram of Dawson (DAWS) shows the strongest negative turning of the X component (-1000 nT), indicating that the substorm electrojet was closest to Dawson. Dawson was also the closest station to local midnight, where most substorms show the strongest magnetic bay signature. As argued in section 3, Polar was most likely in the lobe at onset time. After a rapid expansion of the plasma sheet, Polar reentered the plasma sheet at ~1037 UT, after which it encountered strong electric field fluctuations. The focus of this section is to establish a temporal relationship of Polar's large electric field observations and substorm phases. Figure 9a shows an expanded view of Polar's electric field (E_Z component) from 1000 to 1200 UT on August 29, 1997, together with the magnetic field observations (X component) from Fort McMurray, which we identified as the closest station to Polar's magnetic footpoint. As can be seen, the large electric field fluctuations, lasting for ~5 min in the spacecraft frame, coincided with the expansion phase.

Figure 9b shows the temporal correlation between ground observations and in situ data for another event that took place on April 21, 1997, while Polar's magnetic footpoint traversed the 210 Magnetic Meridian chain on an inbound pass. This substorm showed a 500-nT deflection of the H

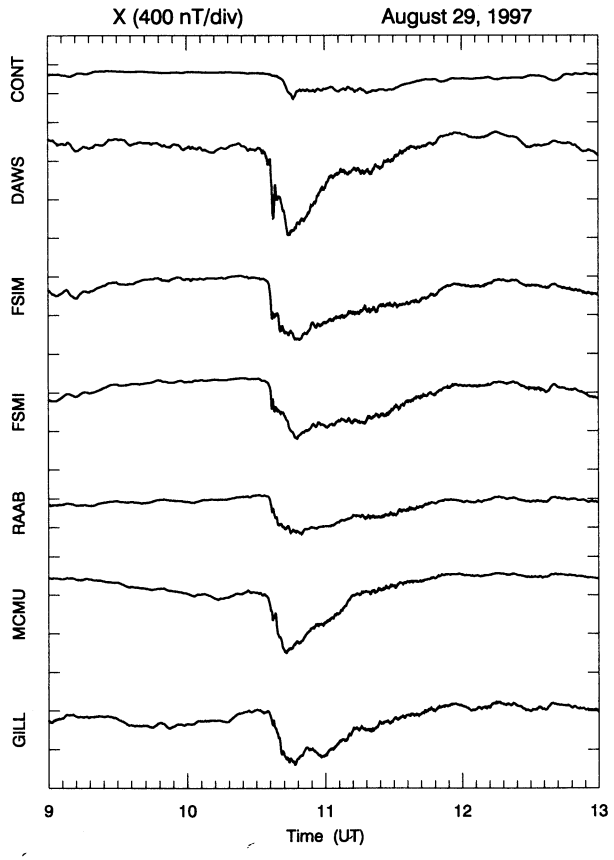

Figure 8. X component of CANOPUS stations. All stations recorded a strong substorm signature (with the exception of CONT), starting at ~1035 UT. The magnetogram at Dawson (DAWS) shows the sharpest negative turning of the X component (~1000 nT), indicating that the substorm electrojet was closest to it.

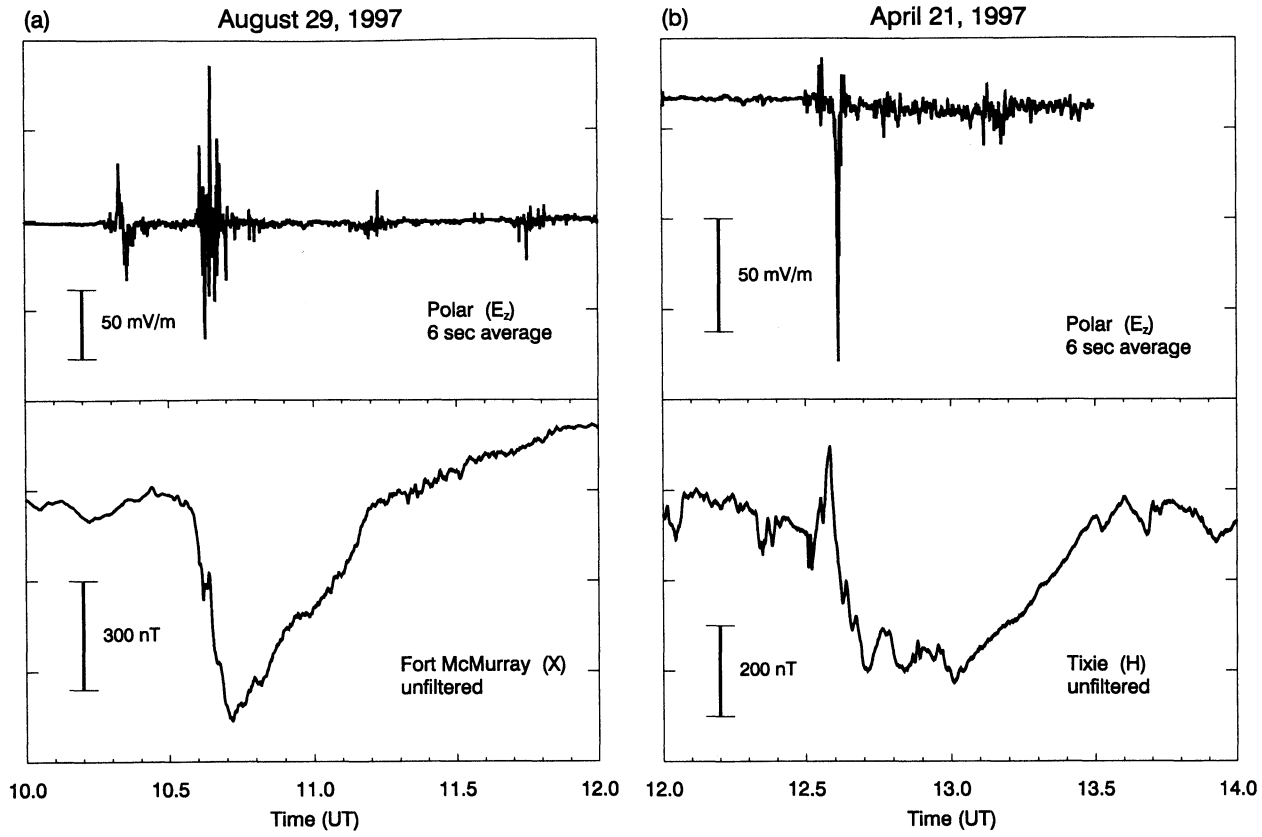

Figure 9. (a) The perpendicular electric field measured by Polar in comparison to the X component measured by the Fort McMurray magnetometer for August 29, 1997. (b) The perpendicular electric field measured by Polar in comparison to the H component measured by the Tixie magnetometer for April, 21, 1997.

component at Tixie. Again, Polar encountered very large perpendicular electric fields at times of strongest H bay deflection. According to Tixie, the onset occurred at ~1235 UT, seen in the sharp negative deflection of H. An earlier deflection of H, at ~1233 UT, was observed at Kotel'nyy (not shown). This onset time agrees with the onset time determined from the AE index.

The good temporal correlation between Polar observations of large perpendicular electric fields and rapid changes in ground magnetic fields as determined from ground stations is further supported in Figure 10, showing the temporal relationship of large perpendicular electric fields measured by Polar and ground magnetometer data for 12 additional substorms. The unfiltered H (or X) component, depending on the magnetometer chain, is presented. The ground stations used and their locations are given in Table 1. The vertical lines indicate the occurrence times of the large electric fields recorded by Polar. The positions of the satellite at those times are shown in Table 2. In all cases the electric fields occurred during times of rapid changes in H (or X), in close temporal proximity to geomagnetic disturbances such as substorm onsets/intensifications. In two events the large

Table 1. Ground Magnetometer Stations used in Figures 9 and 10

Station Name	Magnetometer Array	GLAT, deg	GLON, deg
Gillam	CANOPUS	56.38	265.36
Dawson	CANOPUS	64.05	220.89
Iqaluit	MACCS	63.8	291.5
Pangnirtung	MACCS	66.1	294.2
Tixie	210 MM	65.7	197.1
Kotel'nyy	210 MM	69.9	201.0
Hopen Island	IMAGE	74.02	110.48
Bear Island	IMAGE	71.33	108.73

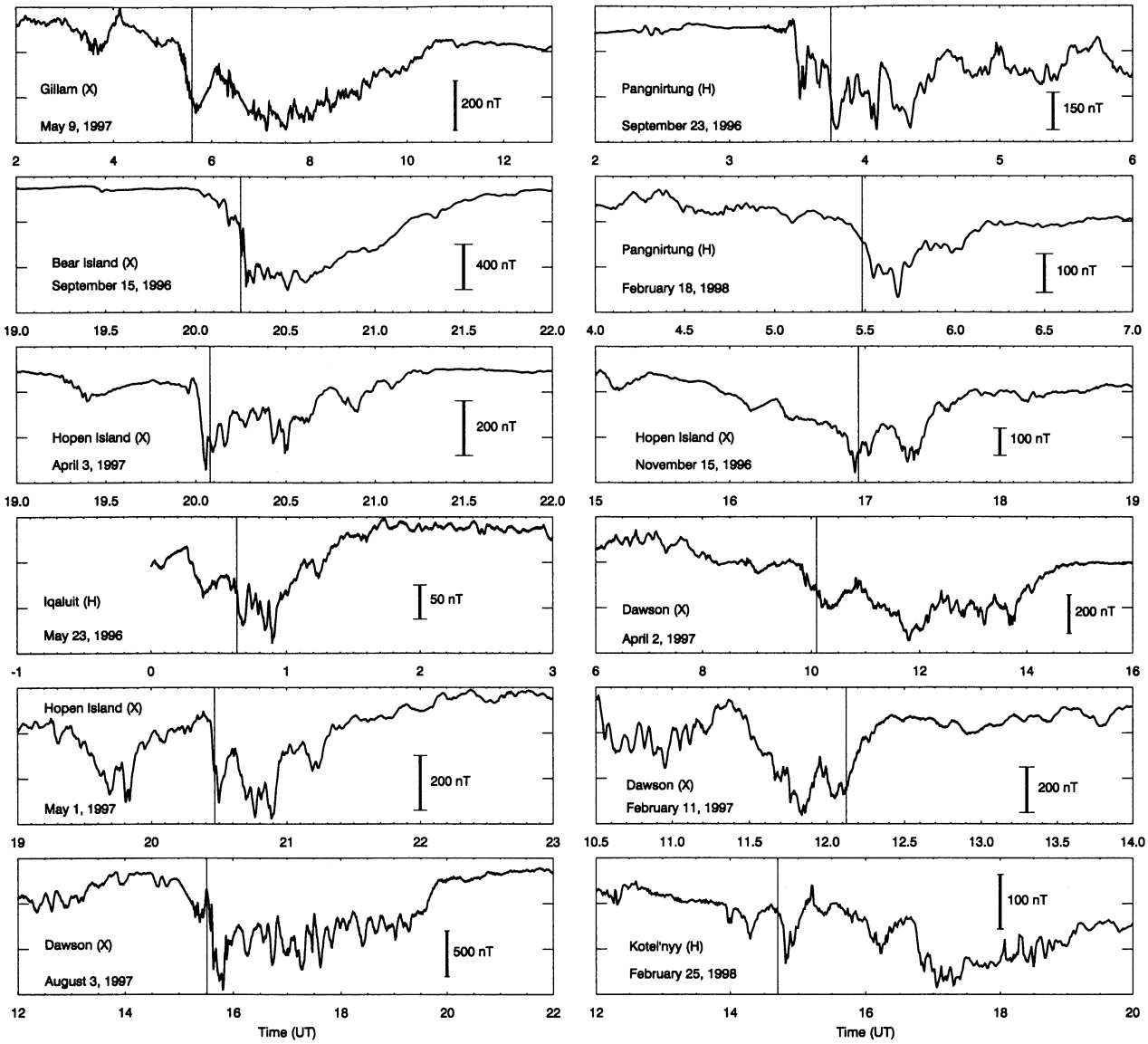

Figure 10. Temporal comparison of large electric field events measured by Polar and ground magnetometer data. Depending on the magnetometer chain, either the unfiltered H or X component is shown. The vertical lines indicate times when Polar observed electric field fluctuations larger than 100 mV m^{-1}. Each panel shows a different substorm/plasma sheet crossing.

Table 2. Polar Ephemeris Data for the Events in Figures 9 and 10

Date	Geocentric Distance	MLT	L Value
May 23, 1996	5.8	2202	9.0
Sept. 15, 1996	5.1	0235	8.6
Sept. 23, 1996	5.0	0230	16.0
Nov. 15, 1996	6.5	2304	17.8
Feb. 11, 1997	5.5	0325	10.0
April 2, 1997	5.1	0005	8.0
April 3, 1997	6.5	0052	12.2
April 21, 1997	5.5	2249	7.8
May 1, 1997	5.2	2320	7.8
May 9, 1997	4.8	2157	9.0
Aug. 3, 1997	4.8	0414	6.0
Aug. 29, 1997	4.6	0242	6.5
Feb. 18, 1998	4.3	0325	8.5
Feb. 25, 1998	4.7	0154	8.5

electric field structure was coincident with a rapid recovery of the H component. Twelve events (including the events in Figure 9) were associated with an expansion (or intensification) phase. An accurate evaluation of whether the event occurred during the downward or upward swing of the H component was complicated for some events because of differences in the ground data from different ground stations that were close to each other.

In the beginning of section 5 it was pointed out that two events occurred during very small values of K_P and AE. One of these events (February 25, 1998) is shown in Figure 10 (last panel). Despite the small activity indices, the event coincided with a negative turning of the H signal at Kotel'nyy station, indicating a disturbed magnetosphere.

5.5. Electromagnetic Signatures

In section 4 it was statistically shown using mapping relationships that high-altitude perpendicular electric fields observed in the nightside plasma sheet were consistent with both the Alfvén wave model and the static model. Alternatively, the nature of perpendicular electric fields can be investigated on the basis of individual events. The E-to-B ratio and phase shifts between E and B are two signatures that are most suited for such an analysis [e.g., *Lysak*, 1998]. In this section we present results regarding the origin of the substorm-related electric fields using E-to-B ratios and phase relationships of the electric and magnetic perturbation fields. We incorporate results from previous case studies which have investigated in greater detail subsets of the large electric field events ($\geq$100 mV m^{-1}) found in this study.

Plate 4 shows two PSBL crossings by Polar during one inbound (April 21, 1997) and one outbound (October 29, 1996) pass. The data for both days are shown in the same format. Plates 4a and 4f show the E_Z component of the electric field which points northward and approximately perpendicular to the nominal plasma sheet boundary (approximately along GSE z). Plates 4b and 4g show the west-east perturbation from the ambient magnetic field (note that in Plate 1 the east-west direction is shown). This component lies approximately in the plane of the nominal plasma sheet. Plates 4c and 4h show the Poynting flux calculated from the three components of the perturbation electric field and the three components of the perturbation magnetic field. These perturbation fields were calculated by detrending each component of the fields. The detrending was done by subtracting a 3-min running average from the original data. The calculated Poynting flux vector was then projected onto the average magnetic field direction. The average magnetic field direction was calculated from the measured magnetic field vector averaged over 3 min. Plates 4d, 4e, 4i, and 4j show the energy spectra of ions and electrons.

The April 21, 1997, lobe-PSBL crossing is characterized by the sharp flux increase of ions and electrons at 1236 UT seen in Plates 4d and 4e. Immediately following the entry, Polar encountered large electric and magnetic field perturbations. The magnetic field perturbation was superimposed on field-aligned currents. The perturbation fields near the lobe-PSBL interface were very similar in waveform with peak amplitudes of -130 mV m^{-1} and -14 nT. The field-aligned Poynting flux associated with these fluctuations (Plate 4c) was directed downward toward the nearest ionosphere. It was largest near the lobe-PSBL interface ($\sim$1 ergs cm^{-2}s^{-1}). The ratio of the peak electric and magnetic field of the perturbation signals is $\sim$9300 km s^{-1}. This is comparable to the local Alfvén speed of $\sim$11,000 km s^{-1} determined from in situ plasma parameters. The correlated electric and magnetic field perturbations are thus consistent with the propagation of Alfvén waves along the magnetic field. Results of a study by A. Keiling et al. (unpublished manuscript, 2000), investigating the spectral composition of the electric and magnetic wave fields of a subset of events (including the April 21, 1997 event), indicate the presence of smaller-amplitude Alfvén waves with a local standing wave structure in both the tail lobe and the PSBL in the Pi2 frequency range. The standing wave structure can be caused by downward traveling Alfvén waves that reflect off at altitudes below the satellite. Poynting flux calculations allow determining the direction of net energy flow. The event on April 21, 1997, clearly shows (Plate 4c) that the earthward component dominates over the reflected one. An example of standing Alfvén waves in the tail lobe can be seen at 1233 UT on April 21, 1997 (Plates 4a and 4b).

The event on October 29, 1996 (Plates 4f-4j), occurred further into the PSBL while Polar was on an outbound pass. Polar entered the PSBL before 0030 UT and entered the tail lobe at $\sim$0100 UT (not shown). The largest electric field pulse ($\sim$190 mV m^{-1}) occurred at $\sim$0037 UT. Shortly thereafter, a smaller electric field pulse ($\sim$70 mV m^{-1}) at $\sim$0038:30 UT was encountered. Both pulses were associated with current sheets of opposite direction. The electron particle flux was reduced between the two pulses; possibly also the ion flux which can only be seen vaguely owing to the limited energy range of the instrument. Immediately preceding the largest electric field pulse is a region of enhanced electron flux. In contrast to the event on April 21, 1997, the electric and magnetic field signals for the event on October 29, 1996, do not show similar waveforms on the scale of 10-60 s. A calculation of the Poynting flux, for the same period range as used for April 21, 1997, also yields large field-aligned Poynting flux ($\geq$0.5 ergs cm^{-2}s^{-1}) directed downward (Plate 4h). The magnetic perturbation of the field-aligned currents largely contributes to this Poynting flux. We emphasize that Poynting flux calculations are strongly dependent on the model subtraction and on the period range chosen for filtering. A separation of a possible Alfvénic contribution requires additional filtering [see, e.g., *Lotko and Streltsov*, 1997]. The identification of the origin of the electric fields for this event is not as unambiguous as in the case of April 21, 1997, and will be further addressed in a forthcoming study.

An inspection of the E-to-B ratio of seven other substorm-related fields, which showed correlated electric and magnetic field signals (including the events in the work of *Wygant et al.* [2000] and *Keiling et al.* [2000]), yields that the ratios

are consistent with wave phase velocities between 8600 and 18,000 km s^{-1}, which is similar to the local Alfvén speed of 12,000-21,000 km s^{-1} determined from plasma measurements. This is evidence on the basis of individual cases, that at least one type of substorm-related electric fields was associated with Alfvén waves. Other events show less correlated signals (e.g., October 29, 1996). Some of these events resemble the DE 1 electric field event investigated by Lotko and Streltsov [1997] (see section 6.3 for further details). In the next section we will comment on the Poynting flux calculation of all 24 events.

5.6. Poynting Flux

In the work of *Keiling et al.* [2000], Poynting flux calculations were presented for a subset of the 24 events. Their selection criterion was that the events showed well-correlated electric and magnetic field signals, and thus an identification of the Alfvénic nature was unambiguous. These events showed large field-aligned Poynting flux, four of which with a clearly dominating earthward component with magnitudes up to 2 ergs $cm^{-2}s^{-1}$. One event (August 29, 1997) showed both large downward and upward Poynting flux. *Keiling et al.* [2000] filtered the data on an individual basis, allowing only the Alfvénic component to contribute to the parallel Poynting flux. In the study presented here we calculated the Poynting flux for all 24 events (in the same way as was done for the previous two events) to estimate the amplitude and direction of the local electromagnetic energy flux regardless of their origin. Thus electromagnetic energy carried by Alfvén waves and field-aligned currents could contribute to the Poynting flux values.

For 21 events the largest parallel Poynting flux component throughout the entire electric field structure associated with each event, which could last up to 5 min, was downward toward the northern ionosphere. Events reported by *Wygant et al.* [2000] and *Keiling et al.* [2000] are included in this statistics. The peak values ranged between 0.3 and 2.5 ergs $cm^{-2}s^{-1}$. When mapped to ionospheric altitudes ($\sim$100 km) along converging magnetic field lines, the Poynting flux would reach magnitudes up to 300 ergs $cm^{-2}s^{-1}$. This is large enough to power very intense auroras. In section 5.4 we showed that the 24 events were associated with geomagnetic disturbances such as substorms. Therefore, the Poynting flux calculations show that large electromagnetic energy flow in the plasma sheet, mostly in the PSBL, is associated with strong geomagnetic disturbances.

6. Discussion

We described results of a statistical survey of perpendicular electric fields recorded during 2 years of Polar operation, consisting of $\sim$940 orbits and $\sim$1880 auroral zone crossings at high altitude in the Northern Hemisphere. The results demonstrate that very large amplitude electric fields perpendicular to the ambient magnetic field occur at geocentric distances of 4-7 R_E. *Wygant et al.* [2000] already reported two of the very large electric field events ($\geq$100 mV m^{-1}) which came from the same database as used in the study presented here. ISEE 1 and 2 are the only other satellites that have traversed the altitude range that was studied in this paper (4-7 R_E geocentric distance in the nightside). There are, however, significant differences to Polar's orbit and instrumentation that make this study relevant. ISEE 1 and 2 were placed in an equatorial orbit. The electric field instrument only contained probes in the equatorial plane and could not measure the component of the electric field perpendicular to the ecliptic and approximately normal to the plasma sheet. In the Polar data set this component was the largest component. In an attempt to characterize perpendicular electric fields in the magnetotail at further distances ($\geq$23 R_E), Geotail studies have also been limited by the fact that the onboard electric field instrument only measures the components in the spin plane, which approximately coincides with the equatorial plane.

6.1. Location of Events

For an understanding of the magnetosphere as a whole, it is important to establish links between different regions in the magnetosphere. In this study it was found that almost all large perpendicular electric fields between 4 and 7 R_E (geocentric distance) occurred on field lines that were magnetically conjugate to the auroral acceleration region. This provides evidence that the electric fields are directly or indirectly related to auroral dynamics. This result allows a direct comparison to previous studies, which presented global distributions of perpendicular electric fields for lower altitudes. *Karlsson and Marklund* [1996], using Freja data, observed the majority of large perpendicular electric field events in the midnight and early morning sectors of the auroral oval in the altitude range from 1400 to 1770 km. *Bennett et al.* [1983] and *Redsun et al.* [1985], using S3-3 data, showed that the largest perpendicular electric field events up to 8000 km altitude tended to occur between 1600 and 2200 MLT. The Polar results reported here show a concentration of the larger electric fields ($\geq$50 mV m^{-1}) around midnight with a few more events in the morning sector. This differs from the S3-3 study, but is similar to the Freja study. However, we point out that the difference between eveningside and morningside in the Polar data set is not statistically significant to confirm a statistical trend.

An additional feature in the Polar distribution is a small concentration of electric fields ($\leq$50 mV m^{-1}) around 1500 MLT, which coincides with the hot spot. The hot spot is a region of increased electron energy flux [*Evans*, 1985] or increased probability of observing electron acceleration events [*Newell et al.*, 1996] inferred from low-altitude satellites. This correspondence further shows the link between electric fields at high-altitude and low-altitude acceleration processes.

A peculiar result, for which we have no definite explanation, is the low event rate at dawn ($\sim$0500 MLT) and dusk ($\sim$1900 MLT). One possibility could be that these regions show the dividing lines between dayside and nightside aurora, which are two different phenomena. The nightside aurora is believed to be magnetically connected to the PSBL

whereas the dayside aurora is connected to the cusp. Hence it seems naturally that there is not a smooth transition between the two regions. If so, it is peculiar, however, that this feature does not appear to some degree in lower-altitude distributions.

6.2. Altitude Dependence

It has been an ongoing issue in auroral physics to discover the origin of large perpendicular electric fields observed on auroral field lines. Two views exist which are physically very different. In one model, the electric fields are interpreted as electrostatic structures, called electrostatic shocks by some researchers. The observed electric and magnetic field fluctuations are caused by the motion of the spacecraft through a system of static field-aligned current structures imbedded in the ionosphere [*Smiddy et al.*, 1980]. The fluctuations are hence entirely caused by the Doppler shift. In the other model, the observed electric fields are the perturbation field of Alfvén waves, which are electromagnetic structures. To help decide this issue, one approach has been to use statistical methods to determine the relationship of electric field magnitudes at different geocentric distances. The assumption of a static model in the form of (2) has been applied to distances far out into the distant magnetotail. *Mozer* [1981], *Levin et al.* [1983], and *Streed et al.* [2000] concluded that the perpendicular electric field magnitudes are not inconsistent with equation (2) out to 7, 23, and 100 R_E, respectively. There is, however, growing evidence in the form of case studies that, at least, some auroral electric fields are Alfvénic [e.g., *Dubinin et al.*, 1990; *Lotko and Streltsov*, 1997; *Wygant et al.*, 2000; *Keiling et al.*, 2000]. Polar data are suitable to investigate the nature of the electric fields both in a statistical analysis, through investigation of possible mapping relationships, and in case studies. The additional use of a statistical study is to make an assessment of many events instead of only a few selected events, which may represent a small class of events. Ideally, one would like to simultaneously measure electric fields along one field line and compare values at different altitudes. Until a multisatellite mission is in place, we rely on statistical analyses to investigate the mapping relationship.

In the first part of the study presented here we compared Polar data to the static model in the form of (1) and (2), and within the range of statistical uncertainties, we confirmed the static model. However, we also showed that the data are consistent with the model in which the observed electric fields are the perturbation fields of shear Alfvén waves, which could be excited on auroral field lines in the distant tail. While propagating toward the ionosphere, the convergent magnetic field focuses the Alfvén wave, and the perturbation electric field magnitude increases. In this case the electric fields do not map quasi-statically along magnetic field lines, and the mapping characteristic of the electric fields was shown to be proportional to $\sqrt{v_A B}$, where v_A is the parallel phase velocity of an Alfvén wave and B is the ambient magnetic field strength. The assumption made is that the power flow, $(A/\mu_0)\delta E \times \delta B$, is constant along the flux tube. At low altitude, i.e., in the inertial regime of Alfvén waves, this will be violated owing to dissipation processes (e.g., particle acceleration) and wave dispersion (kinetic Alfvén waves, finite $k_\perp$) [*Lotko and Streltsov*, 1997]. The importance of our result is that it removes one objection against the Alfvén wave model, and that it statistically shows that Alfvén waves could be a very common occurrence on auroral field lines, forming the majority of large-amplitude perpendicular electric fields ($\geq$20 mV m^{-1}). Earlier statistical studies covering the same region did not attempt to show whether their data were also consistent with Alfvén waves.

Polar data can be consistent with both the static model and the shear Alfvén wave model, because the average Alfvén speed between 4 and 7 R_E varies by only a factor of 2 to 3. This variation is not large enough to separate the models given the statistical uncertainties. This is also true for distances further than 7 R_E. Hence, if (3) were applied to ISEE 1 data [e.g., *Mozer*, 1981; *Levin et al.*, 1983], the results would be inconclusive as well. The theoretical Alfvén speed profile from the ionosphere to the equatorial plane along a magnetic field line [e.g., *Streltsov and Lotko*, 1997, Figure 1] shows that the largest change in v_A (a factor of 40-50) occurs around 1 and 3 R_E geocentric distance. This region, however, overlaps with the auroral acceleration region in which field-aligned potential drops occur. Hence, one would not expect the simple relation (3) to hold in this region.

Furthermore, note that both the static model and the shear Alfvén wave model applied in this study contain the implicit assumption that electric fields on the same magnetic field line are related. Therefore the consistency of Polar data with both models, together with the distribution in ILAT and MLT of electric field events (Plate 2), is strong evidence that perpendicular electric fields on auroral field lines at various altitudes are indeed related to one another. Polar's high-altitude observations are thus related to the large-amplitude perpendicular electric fields, routinely observed in the auroral acceleration region, which are believed to be responsible for discrete auroral arcs [e.g., *Torbert and Mozer*, 1978; *Kletzing et al.*, 1983; *Lyons*, 1991].

6.3. Substorm-Related Electric Fields

In a further attempt to characterize auroral perpendicular electric fields, we investigated the largest electric fields ($|E_Z| \geq$100 mV m^{-1}) found during the 2-year time period of the statistical study with regard to polarization, plasma regime, association with field-aligned currents, electromagnetic signature, Poynting flux, and geomagnetic activity. In 24 crossings out of ~940 orbits, 24 electric fields of perpendicular magnitude greater than 100 mV m^{-1} (6 s averaged) were found.

The electric field structures of the events were polarized dominantly north-south when mapped down to the ionosphere. Observations of large perpendicular electric fields at low altitudes, made with the Freja satellite, also showed dominantly north-south polarization [*Marklund et al.*, 1995], giving further evidence (in addition to location and altitude dependence) that the large events presented here are related

to low-altitude events. Bearing in mind the difficulties of identifying the plasma regime associated with some of the large electric fields, we concluded that ~85% of the events occurred at or near the poleward edge of the PSBL. The remaining events occurred deeper inside the CPS. An ISEE 1 study covering the range from 7 to 23 R_E found similar results with the exception that the authors associated all of their events with the PSBL [*Cattell et al.*, 1982].

Our study shows that very large, dominantly north-south polarized fields in the magnetotail were directly correlated with the rapid changes in the H (or X) component of ground magnetometer records indicating the occurrence of geomagnetic disturbances such as substorms. Although other studies [*Nishida et al.*, 1983; *Aggson et al.*, 1983; *Cattell and Mozer*, 1984; *Pedersen et al.*, 1985; *Smits et al.*, 1986; *Maynard et al.*, 1996] have identified large perpendicular electric fields during times of substorms, these observations differ from our observations in location and polarization of the electric fields. It was reported that they occurred close to the equatorial plane within 20 R_E and were polarized in the dawn-dusk direction. These fields were attributed to either enhanced convection or dipolarization, none of which is a likely generation mechanism for the fields reported here. For one substorm event observed by ISEE 1 and 2, *Kelly et al.* [1984] reasoned that plasma flow in the azimuthal (west-east) direction, embedded in a current sheet, could account for the observed large, north-south polarized electric fields. For a large fraction of events ($\leq$50%) presented here, the E-to-B ratio of the two perturbation fields was consistent with Alfvén waves. Some of the events did not show a good correlation between the electric and magnetic fields, at least for the 10-60 period fluctuations considered here. In these cases the intense electric fields often occurred at the edge of a field-aligned current sheet, which resembles more an electrostatic structure. Some of these events resemble the DE 1 electric field event investigated by *Lotko and Streltsov* [1997]. The authors argued that in a specified frequency range, the event exhibits the waveform and phase structure of a dispersive field line resonance.

Poynting flux calculations have demonstrated that the majority of events (21 events) were associated with strong Poynting fluxes up to 2.5 ergs $cm^{-2}s^{-1}$, directed downward along the background magnetic field into the ionosphere. If this Poynting flux reached the ionosphere, its magnitude would exceed 300 ergs $cm^{-2}s^{-1}$ owing to converging magnetic field lines. This would be sufficient to power the most intense auroras.

6.4. Occurrence Frequency

Having shown that the largest perpendicular electric fields ($\geq$100 mV m^{-1}) investigated in this study occurred during the expansion/intensification phase, it is important to investigate whether every substorm is accompanied by large electric fields like the ones shown in this study. This issue can be addressed in a probabilistic manner. Since substorms occur ~4 or 5 times a day, those fields should occur a significant fraction of time. During a period of 2 years, only a total of 24 events were observed. Although this is a small number, it must be realized that Polar spends most of its time outside the plasma sheet. Alternatively, it was shown that the substorm-related electric fields ($\geq$100 mV m^{-1}) occurred with a probability of 2-4% per plasma sheet crossing in the nightside. Considering that a Polar plasma sheet crossing takes ~30-60 min and large electric fields occur closer to the poleward edge of the plasma sheet, 2-4% represents a significant fraction of time. If we allow for substorm-related electric fields less than 100 mV m^{-1} (for which we also have evidence), the probability of encountering these fields will increase. For example, we showed that events with electric fields larger than 50 mV m^{-1} occurred with a 15% probability. On the other hand, the probability that an expansion phase occurs while Polar is in the plasma sheet varies between 8 and 20%. This rough calculation is based on the Polar plasma sheet crossing time of 30-60 min and the assumption that 4-5 substorms occur per day, with the expansion/intensification phase being treated as a single event. Hence the occurrence frequency of electric fields larger than 50 mV m^{-1} is comparable to the substorm occurrence frequency, which suggests that north-south polarized, large electric fields might be generally correlated with the substorm expansion/intensification phase. Naturally, this is only a rough comparison. The argumentation given here is only suggestive and requires further investigation.

In a study by *Karlsson and Marklund* [1996], it was shown that large perpendicular electric fields at low altitude do not depend on the level of geomagnetic activity inferred from the K_P index. This is, however, not necessarily inconsistent with the above comparison, because smaller-scale geomagnetic disturbances such as, for example, pseudobreakups [*Koskinen et al.*, 1993] can also manifest themselves in ground data but are not necessarily detected with the coarse K_P index. In fact, we found that in spite of very small K_P values during the occurrence of some intense electric fields, geomagnetic disturbances were nevertheless recorded at individual ground stations.

7. Conclusions

The survey of 2 years of Polar high-altitude perpendicular electric field data resulted in the following conclusions (only the E_Z component was investigated for this part of the study):

1. Large electric fields perpendicular to both the magnetic field and the plane of the nominal plasma sheet at 4-7 R_E can exceed 100 mV m^{-1}.

2. Almost all electric field events ($\geq$20 mV m^{-1}) were found within the statistical location of the auroral oval with a few events occurring inside the statistical location of the polar cap. The distribution along the auroral oval was not uniform. The largest electric fields occurred more often around local midnight. The dayside events were less intense than the nightside events. On the dayside a small concentration of electric fields existed at ~1500 MLT, which coincides with the so-called hot spot. There were two 2-hour wide regions

on the dawnside (~0500 MLT) and duskside (~1900 MLT) which showed significantly lower event rates than the surrounding regions.

3. The magnitude-versus-altitude distribution is consistent with both a static model and a shear Alfvén wave model. We regard this as new support for the Alfvén wave model, which means that Alfvén waves (being a common feature on auroral field lines) could, in principle, account for the majority of electric field observations for small and large amplitudes.

4. The occurrence frequency of electric field events decreased monotonically with increasing magnitude.

The second part of this study focused on individual events selected from the statistical database. The selection criterion was that the amplitude of the E_Z component exceeded 100 mV m^{-1}. Over the entire period of 2 years, 24 events were found. The important results regarding the largest electric fields are summarized as follows:

1. About 85% of the events occurred in the vicinity of the outer boundary of the plasma sheet; the remaining events occurred further into the plasma sheet (CPS).

2. The location of the outer boundary of the plasma sheet ranged from 65° to 78° ILAT for the plasma sheet crossings associated with the 24 events.

3. The events occurred in regions of large-scale field-aligned currents.

4. The polarity of the electric fields was dominantly in the north-south direction, perpendicular to the nominal plasma sheet boundary.

5. The events occurred with a 2-4% probability per Polar plasma sheet crossing.

6. For a large fraction ($\leq$50%) the ratio of electric and magnetic fields yielded wave phase velocities of 8600-18,000 km s^{-1}, which was in the range of the local Alfvén velocity of 12,000 to 21,000 km s^{-1}.

7. A majority of the events (21 events) was associated with large field-aligned Poynting flux (~1 ergs cm^{-2}s^{-1}) directed downward into the Northern Hemisphere ionosphere.

8. For 14 events it was shown that they occurred during times of rapid changes in the H (or X) component of ground magnetometer data in close temporal proximity to geomagnetic disturbances such as substorm onset/intensification. For the remaining events it was found that they also occurred during active times determined from the AE index.

From these results it is evident that large perpendicular electric fields ($\geq$20 mV m^{-1}) observed on auroral field lines are related, although, on the basis of the statistical part of this study, we can not conclusively decide of what origin they are. However, beside the often quoted electrostatic model to explain the bulk of auroral electric fields, it was statistically shown, for the first time at altitudes between 4 and 7 R_E, that the Alfvén wave model cannot be ruled out as a possible generation mechanism. Despite the ambiguity of the statistical study, we can conclude, on the basis of the E-to-B ratio and the phasing relationship of the electric and magnetic perturbation fields for individual events, that a large fraction of the largest events ($\geq$100 mV m^{-1}) are the perturbation fields of Alfvén waves. The other events require further investigation. Poynting flux calculations for the 24 events indicate that there is a clear dominance of downward field-aligned Poynting flux. This result is in agreement with *Wygant et al.* [2000], *Keiling et al.* [2000], and *Toivanen et al.* [2000]. We also demonstrated that the largest events ($\geq$100 mV m^{-1}) occurred during the expansion (or intensification) phase, and thus there is further evidence that electromagnetic energy transfer processes occur during the most dynamic phase of geomagnetic disturbances.

Acknowledgments. Analysis of electric field data was supported by NASA International Solar Terrestrial Program (NASA contract NAG 5-3182). Analysis of magnetometer data was supported by NASA ISTP grant 5-3217. Work at the University of Iowa in analysis of Hydra data was performed under NASA grant 5-2231 and DARA grant 50 OC 8911 0. The IMAGE magnetometer data are collected as a Finnish-German-Norwegian-Polish-Russian-Swedish project. We thank Ari Viljanen from the Finnish Meteorological Institute for the IMAGE data. The CANOPUS project is supported by the Canadian Space Agency. We thank John Samson for the CANOPUS data. We thank Mark Engebretson for providing MACCS data. The MACCS array was supported by NSF grant ATM-9610072 to Augsburg College and ATM-9704766 to Boston University. We also thank all members of the 210 MM Magnetic Observation Group for their ceaseless support. The database of the 210 MM project is made at STEL, Nagoya University. We would also like to thank Reiner Friedel and coworkers for use of the PAPCO graphical display program.

Hiroshi Matsumoto thanks L.R. Lyons and G.T. Marklund for their assistance in evaluating this paper.

References

Aggson, T.L., J.P. Heppner, and N.C. Maynard, Observations of large magnetospheric electric fields during the onset phase of a substorm, *J. Geophys. Res., 88,* 3981-3990, 1983.

Baker, D.N., T.I. Pulkkinen, V. Angelopoulos, W. Baumjohann, and R.L. McPherron, Neutral line model of substorms: Past results and present view, *J. Geophys. Res., 101,* 12,975-13,010, 1996.

Baumjohann, W., G. Paschmann, and T. Nagai, Thinning and expansion of the substorm plasma sheet, *J. Geophys. Res., 97,* 17,173-17,175,1992.

Bennett, E.L., M. Temerin, and F.S. Mozer, The distribution of auroral electrostatic shocks below 8000-km altitude, *J. Geophys. Res., 88,* 7107-7120, 1983.

Cattell, C.A., M. Kim, R.P. Lin, and F.S. Mozer, Observations of large electric fields near the plasma sheet boundary by ISEE-1, *Geophys. Res. Lett., 9,* 539-542,1982.

Cattell, C.A., and F.S. Mozer, Substorm electric fields in the Earth's magnetotail, in *Magnetic Reconnection in Space and Laboratory Plasmas, Geophys. Monogr. Ser.*, vol. 30, edited by E.W. Hones, Jr., pp. 208-215, AGU, Washington, D.C., 1984.

Cattell, C.A., F.S. Mozer, K. Tsuruda, H. Hayakawa, M. Nakamura, T. Okada, S. Kokubun, and T. Yamamoto, Geotail observations of spiky electric fields and low-frequency waves in the plasma sheet and plasma sheet boundary, *Geophys. Res. Lett., 21,* 2987-2990, 1994.

Dubinin, E.M., P.L. Israelevich, and N.S. Nikolaeva, Auroral electromagnetic disturbances at an altitude of 900 km: The relationship between the electric and magnetic field variations, *Planet. Space Sci., 38,* 97-108, 1990.

Evans, D.S., The characteristics of a persistent auroral arc at high latitude in the 1400 MLT sector, in The Polar Cusp, edited by J.A. Holtet and A. Egeland, pp. 99-107, D. Reidel, Norwell, Mass., 1985.

Goertz, C.K., Kinetic Alfvén waves on auroral field lines, *Planet. Space Sci., 32,*, 1387-1392, 1984.

Gurnett, D.A., R.L. Huff, J.D. Menietti, J.L. Burch, J.D. Winning-

ham, and S.D. Shawhan, Correlated low-frequency electric and magnetic noise along the auroral field lines, *J. Geophys. Res., 89,* 8971-8985, 1984.

Harvey, P., et al., The electric field instrument on the Polar satellite, in *The Global Geospace Mission*, edited by C.T. Russell, pp. 583-596, Kluwer Acad., Norwell, Mass., 1995.

Hasegawa, A., Particle acceleration by MHD surface wave and formation of aurora, *J. Geophys. Res., 81,* 5083-5090, 1976.

Karlsson, T., and G.T. Marklund, A statistical study of intense low-altitude electric fields observed by Freja, *Geophys. Res. Lett., 23,* 1005-1008, 1996.

Keiling, A., J.R. Wygant, C.A. Cattell, M. Temerin, F.S. Mozer, C.A. Kletzing, J.D. Scudder, C.T. Russell, W. Lotko, and A.V. Streltsov, Large Alfvén wave power in the plasma sheet boundary layer during the expansion phase of substorms, *Geophys. Res. Lett., 27,* 3169-3172, 2000.

Kelly, T.J., C.T. Russell, and R.J. Walker, ISEE 1 and 2 observations of an oscillating outward moving current sheet near midnight, *J. Geophys. Res., 89,* 2745-2754, 1984.

Kletzing, C., C. Cattell, F.S. Mozer, S.-I. Akasofu, and K. Makita, Evidence for electrostatic shocks as the source of discrete auroral arcs, *J. Geophys. Res., 88,* 4105-4113, 1983.

Koskinen, H.E.J., R.E. Lopez, R.J. Pellinen, T.I. Pulkinen, D.N. Baker, and T. Bosinger, Pseudo-breakups and substorm growth phase in the ionosphere and magnetosphere, *J. Geophys. Res., 98,* 5801-5813, 1993.

Levin, S., K. Whitley, and F.S Mozer, A statistical study of large electric field events in the Earth's magnetotail, *J. Geophys. Res., 88,* 7765-7768, 1983.

Lindqvist, P.-A., and G.T. Marklund, A statistical study of high-altitude electric fields measured on the Viking satellite, *J. Geophys. Res., 95,* 5867-5876, 1990.

Lotko, W., and A.V. Streltsov, Magnetospheric resonance, auroral structure and multipoint measurements, *Adv. Space Res., 20* (4/5), 1067-1073, 1997.

Lyons, L.R., Discrete auroras and magnetotail processes, in *Auroral Physics,* edited by C.-I. Meng, M.J. Rycroft, and L. A. Frank, pp.195-205, Cambridge Univ. Press, New York, 1991.

Lysak, R., The relationship between electrostatic shocks and kinetic Alfvén waves, *J. Geophys. Res., 25,* 2089-2092, 1998.

Mallinckrodt, A.J., and C.W. Carlson, Relations between transverse electric fields and field-aligned currents, *J. Geophys. Res., 83,* 1426-1432, 1978.

Marklund, G.T., L.G. Blomberg, P.-A. Lindqvist, and L. Eliasson, On the occurrence of intense low-altitude electric fields observed by Freja, *Ann. Geophys. 13,* 704, 1995.

Maynard, N.C., W.J. Burke, E.M. Basinska, G.M. Erickson, W.J. Hughes, H.J. Singer, A.G. Yahnin, D.A. Hardy, and F.S. Mozer, Dynamics of the inner magnetosphere near times of substorm onset, *J. Geophys. Res., 101,* 7705-7736, 1996.

Mozer, F.S, Magnetospheric dc electric fields: Present knowledge and outstanding problems to be solved during the IMS, in *The Scientific Programme During the International Magnetospheric Study*, pp. 101-131, D. Reidel, Norwell, Mass., 1976.

Mozer, F.S., ISEE-1 observations of electrostatic shocks on auroral zone field lines between 2.5 and 7 Earth radii, *Geophys. Res. Lett., 8,* 823-826, 1981.

Mozer, F.S., et al., Observations of paired electrostatic shocks in the polar magnetosphere, *Phys. Rev. Lett., 38,* 292-295, 1977.

Newell, P.T., K.M. Lyons, and C.-I. Meng, A large survey of electron acceleration events, *J. Geophys. Res., 101,* 2599-2614, 1996.

Nishida, A., Y.K. Tulunay, F.S. Mozer, C.A. Cattell, E.W. Hones, and J. Birn, Electric field evidence for tailward flow at substorm onset, *J. Geophys. Res., 88,* 9109-9113, 1983.

Parks, G.K., et al., Particle and field characteristics of the high-latitude plasma sheet boundary layer,, *J. Geophys. Res., 89,* 8885-8906, 1984.

Pedersen, A., C.A. Cattell, C.-G. Falthammer, K. Knot, P.-A. Lindqvist, R.H. Manka, and F.S. Mozer, Electric fields in the plasma sheet and plasma sheet boundary layer, *J. Geophys. Res., 90,* 1231-1242, 1985.

Redsun, M.S., M. Temerin, and F.S Mozer, Classification of auroral electrostatic shocks by their ion and electron associations, *J. Geophys. Res., 90,* 9615-9633, 1985.

Reiff, P.H., G. Lu, J.L. Burch, J.D. Winningham, L.A. Frank, J.D. Craven, W.K. Peterson, and R.A. Heelis, On the high- and low-altitude limits of the auroral electric field region, in *Auroral Plasma Dynamics, Geophys. Monogr. Ser.,* vol.80, edited by R.L. Lysak, pp.143-154, AGU, Washington, D.C., 1993.

Russell, C.T., R.C. Snare, J.D. Means, D. Pierce, D. Dearborn, M. Larson, G. Barr, and G. Le, The GGS/Polar Magnetic Fields Investigation, in *The Global Geospace Mission*, edited by C.T. Russell, pp. 563-582, Kluwer Acad., Norwell, Mass., 1995.

Scudder, J., et al., Hydra: A 3-dimensional electron and ion hot plasma instrument for the Polar spacecraft of the GGS mission, in *The Global Geospace Mission,* edited by C.T. Russell, pp. 459-495, Kluwer Acad., Norwell, Mass., 1995.

Smiddy, M., W.J. Burke, M.C. Kelley, N.A. Saflekos, M.S. Gussenhoven, D.A. Hardy, and F.J. Rich, Effects of high-latitude conductivity on observed convection electric fields and Birkeland currents,, *J. Geophys. Res., 85,* 6811-6818, 1980.

Smits, D.P., W.J. Hughes, C.A. Cattell, and C.T. Russell, Observations of field-aligned currents, waves, and electric fields at substorm onset, *J. Geophys. Res., 91,* 121-134, 1986.

Streed, T., C. Cattell, F. Mozer, S. Kokubun, and K. Tsuruda, Spiky electric fields in the magnetotail, *J. Geophys. Res.,* in press, 2000.

Streltsov, A.V., and W. Lotko, Dispersive, nonradiative field line resonances in a dipolar magnetic field geometry, *J. Geophys. Res., 102,* 27,121-27,135, 1997.

Torbert, R.B., and F.S. Mozer, Electrostatic shocks as the source of discrete auroral arcs, *Geophys. Res. Lett., 5,* 135-138, 1978.

Toivanen, P.K., D.N. Baker, W.K. Peterson, X. Li, E.F. Donovan, A. Viljanen, A. Keiling, and J.R. Wygant, Plasma sheet dynamics observed by the Polar spacecraft in association with substorm onsets, *J. Geophys. Res.,* in press, 2000.

Weimer, D.R., and D.A. Gurnett, Large-amplitude auroral electric fields measured with DE 1, *J. Geophys. Res., 98,* 13,557-13,564, 1993.

Winningham, J.D., and W.J. Heikkila, Polar cap auroral electron fluxes observed with ISIS 1, *J. Geophys. Res., 79,* 949-957, 1974.

Wygant, J.R., et al., Polar spacecraft based comparison of intense electric fields and Poynting flux near and within the plasma sheet-tail lobe boundary to UVI images: An energy source for the Aurora, *J. Geophys. Res., 105,* 18,675-18,692, 2000.

Yumoto, K., and the 210 degree MM magnetic observation group, The STEP 210 degree magnetic meridian network project, *J. Geomagn. Geoelectr., 48,* 1297-1309, 1996.

C. Cattell, M. Johnson, A. Keiling, and J. R. Wygant, School of Physics and Astronomy, University of Minnesota, 116 Church St. S.E., Minneapolis, MN 55455. (akeiling@ham.space.umn.edu)

F. S. Mozer and M. Temerin, Space Sciences Laboratory, University of California, Berkeley, CA 94720.

C. A. Kletzing and J. Scudder, Physics Department, University of Iowa, Iowa City, IA 52242.

C. T. Russell, IGPP, University of California, Los Angeles, CA 90024.

(Received May 11, 2000; revised September 8, 2000; accepted September 8, 2000.)